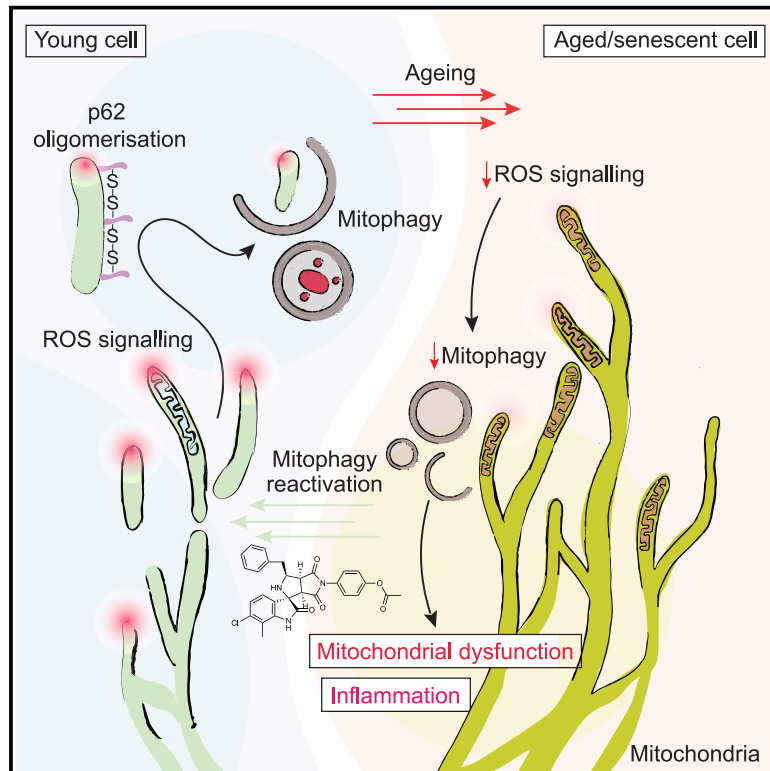# Developmental Cell

Suppressed basal mitophagy drives cellular aging phenotypes that can be reversed by a p62-targeting small molecule

Graphical abstract

Authors

George Kelly, Tetsushi Kataura, Johan Panek, ..., Bernadette Carroll, Jóhannes Reynisson, Viktor I. Korolchuk

Correspondence

viktor.korolchuk@newcastle.ac.uk

In brief

Kelly and Kataura et al. demonstrate that basal quality control of mitochondria by mitophagy in primary human cells is mediated by the PINK1/Parkin/p62 pathway. Declining activity of mitophagy was shown to drive an array of cellular aging phenotypes, and reactivation of mitophagy was sufficient to reverse these changes.

Highlights

- Basal mitophagy is highly active in various primary human cells in culture
- PINK1, Parkin, and p62 are essential for basal mitophagy in primary fibroblasts
- Loss of mitophagy drives cellular senescence phenotypes and is evident in aging
- Mitophagy activators rescue senescence/aging-related changes in cell function

CellPress

Developmental Cell

Article

Suppressed basal mitophagy drives cellular aging phenotypes that can be reversed by a p62-targeting small molecule

George Kelly,[1,14] Tetsushi Kataura,[1,2,14] Johan Panek,[1] Gailing Ma,[1] Hanna Salmonowicz,[3] Ashley Davis,[1] Hannah Kendall,[4] Charlotte Brookes,[1] Daniel Moscoh Ayine-Tora,[5] Peter Banks,[1] Glyn Nelson,[1] Laura Dobby,[1,13] Patricia R. Pitrez,[6] Laura Booth,[7] Lydia Costello,[8] Gavin D. Richardson,[1] Penny Lovat,[9] Stefan Przyborski,[8] Lino Ferreira,[6] Laura Greaves,[4] Karolina Szczepanowska,[3] Thomas von Zglinicki,[1] Satomi Miwa,[1] Max Brown,[10] Michael Flagler,[10] John E. Oblong,[10] Charles C. Bascom,[10] Bernadette Carroll,[11] Jóhannes Reynisson,[12] and Viktor I. Korolchuk[1,15,*]

[1]Biosciences Institute, Faculty of Medical Sciences, Newcastle University, Newcastle upon Tyne NE4 5PL, UK
[2]Department of Neurology, Institute of Medicine, University of Tsukuba, Tsukuba, Ibaraki 305-8575, Japan
[3]ReMedy International Research Agenda Unit, IMol Polish Academy of Sciences, Warsaw 02-247, Poland
[4]Wellcome Centre for Mitochondrial Research, Biosciences Institute, Faculty of Medical Sciences, Newcastle University, Newcastle upon Tyne NE2 4HH, UK
[5]Department of Chemistry, University of Ghana, LG 56, Legon-Accra, Ghana
[6]FMUC – Faculty of Medicine, Pólo das Ciências da Saúde, Unidade Central Azinhaga de Santa Comba, Coimbra 3000-354, Portugal
[7]Translation and Clinical Research Institute, Newcastle University, Newcastle upon Tyne NE2 4HH, UK
[8]Department of Biosciences, Durham University, Durham DH1 3LE, UK
[9]Precision Medicine, Translation and Clinical Research Institute, Newcastle University Centre for Cancer, The Medical School, Framlington Place, Newcastle upon Tyne NE2 4HH, UK
[10]The Procter & Gamble Company, Cincinnati, OH 45040, USA
[11]School of Biochemistry, University of Bristol, Bristol BS8 1TD, UK
[12]School of Pharmacy and Bioengineering, Keele University, Newcastle under Lyme ST5 5BG, UK
[13]Present address: Centre for Bacterial Cell Biology, Biosciences Institute, Faculty of Medical Sciences, Newcastle University, Newcastle upon Tyne NE2 4AX, UK
[14]These authors contributed equally
[15]Lead contact
*Correspondence: viktor.korolchuk@newcastle.ac.uk
https://doi.org/10.1016/j.devcel.2024.04.020

SUMMARY

Selective degradation of damaged mitochondria by autophagy (mitophagy) is proposed to play an important role in cellular homeostasis. However, the molecular mechanisms and the requirement of mitochondrial quality control by mitophagy for cellular physiology are poorly understood. Here, we demonstrated that primary human cells maintain highly active basal mitophagy initiated by mitochondrial superoxide signaling. Mitophagy was found to be mediated by PINK1/Parkin-dependent pathway involving p62 as a selective autophagy receptor (SAR). Importantly, this pathway was suppressed upon the induction of cellular senescence and in naturally aged cells, leading to a robust shutdown of mitophagy. Inhibition of mitophagy in proliferating cells was sufficient to trigger the senescence program, while reactivation of mitophagy was necessary for the anti-senescence effects of NAD precursors or rapamycin. Furthermore, reactivation of mitophagy by a p62-targeting small molecule rescued markers of cellular aging, which establishes mitochondrial quality control as a promising target for anti-aging interventions.

INTRODUCTION

Macroautophagy (hereafter referred to as autophagy) is a bulk cellular recycling process induced upon starvation to degrade cytosolic macromolecules while also being involved in the selective degradation of damaged cellular components such as protein aggregates and dysfunctional organelles. Targeting of autophagy cargo to the nascent autophagosome (called phagophore) is dependent on a family of selective autophagy receptors

(SARs).[1] These proteins are typically characterized by their ability to bind both ubiquitinated cargo and autophagy proteins. This tethering and scaffolding function of SARs allows phagophore(s) to expand around the cargo and seal to form an autophagosome, followed by fusion with lysosomes where the cargo is degraded and the content is recycled.[1]

Selective autophagic clearance of mitochondria (mitophagy) is increasingly recognized as a key cellular quality control mechanism, perturbation of which may contribute to the development

CellPress
OPEN ACCESS

Developmental Cell
Article

of age-related diseases.[2,3] PTEN-induced putative kinase (PINK1)/Parkin-mediated mitophagy is arguably the most studied selective autophagy pathway to date.[4] PINK1 is a protein kinase that accumulates at the outer membrane of damaged mitochondria, specifically those characterized by the loss of membrane potential. Stabilization of PINK1 allows it to phosphorylate several downstream targets, including the E3 ubiquitin ligase Parkin and ubiquitin itself. Ubiquitination of mitochondrial surface proteins by Parkin in turn initiates a cascade of molecular events leading to the engulfment and sequestration of the damaged mitochondrion by a newly formed autophagosome.[4] Damage-induced mitophagy involves the binding of SARs to the ubiquitinated mitochondria. The SARs, optineurin (OPTN), calcium binding and coiled-coil domain 2 (CALCOCO2/NDP52), Tax1 binding protein 1 (TAX1BP1), NBR1 autophagy cargo receptor (NBR1), and sequestosome 1 (SQSTM1/p62) have all been shown to be recruited to damaged mitochondria; however, only OPTN, NDP52, and, to a lesser extent, TAX1BP1 were found to be required for mitophagy.[5] Mitophagy receptors in turn trigger the chain reaction of protein-protein interactions primarily to attract, in a rapid and efficient manner, the autophagy initiation machinery, which ultimately builds an autophagic vesicle marked by microtubule-associated protein 1 light chain 3 (LC3)-family proteins.[4]

The molecular mechanisms of the PINK1/Parkin mitophagy pathway have, so far, been elucidated in models of excessive mitochondrial damage, for example, using the ionophore carbonyl cyanide 3-chlorophenylhydrazone (CCCP) to dissipate mitochondrial membrane potential ($\Delta\psi m$) or respiratory complex inhibitors antimycin and oligomycin.[5] However, mechanisms of basal mitophagy in unstressed cells and the contribution of the PINK1/Parkin pathway to this process are not only poorly understood but frequently disputed.[6,7] This could, at least in part, be attributed to the fact that the basal rates of mitophagy are extremely low in commonly studied, immortalized cell models.[5,8–10] As such, it has not been possible to assess the importance of mitophagy for cellular physiology despite its predicted role in the maintenance of mitochondrial quality control and cellular function.[2] Based on our indirect assessments of mitophagy in primary human fibroblasts, we have previously proposed that mitophagy dysfunction could be an important mechanism in the development of cellular senescence.[11,12]

Cellular senescence is triggered by irreparable damage, resulting in a permanent cell cycle arrest. The mechanisms leading to senescence acquisition are complex, and the key drivers that activate the senescence program remain unclear. Senescent cells are typically characterized by a set of markers such as persistent DNA damage, elevated levels of reactive oxygen species (ROS), increased cell size with an expansion of cellular organelles including the nucleus and lysosomal compartment (the latter visualized by the senescence-associated β-galactosidase [SA-β-GAL] staining), and senescence-associated secretory phenotype (SASP).[12] Significant alterations to mitochondrial network are also observed; however, they are still vastly underexplored. Our knowledge is limited to the observations of massive expansion of mitochondria, mitochondrial network hyper-fusion, and ultimately inefficient respiration.[13] Cellular senescence has now emerged as an important element of organismal aging, which is associated with a gradual accumulation of senescent cells in various tissues that has been shown to

contribute to the age-related functional decline.[14] As such, understanding the mechanisms controlling the transition of cells to the senescent state is essential for the development of therapeutic strategies aiming to slow down aging.

Here, we capitalized on our discovery of high levels of basal mitophagy in primary human cells to investigate both the mechanisms controlling mitophagy as well as its role in cells without the application of mitochondrial toxins.[5,8] By focusing on human dermal fibroblasts, our studies delineated the triggers and the molecular players maintaining basal mitophagy. Furthermore, we discovered that mitophagy is downregulated in response to senescence stimuli and in cells from aged donors, identifying this event as a driver of the cellular aging phenotypes. Taken together, our data indicate that mitophagy may represent a promising target for the development of anti-aging strategies.

RESULTS

Mitophagy suppression is an early event during senescence acquisition

Loss of mitochondrial turnover by autophagy can contribute to an accumulation of dysfunctional mitochondria, which is a key feature of senescent cells.[12] We therefore hypothesized that mitophagy dysregulation may play an important role in cellular senescence and aging. To test this, we generated primary neonatal human diploid fibroblasts (HDFs) stably expressing a mitophagy reporter, mt-mKeima. mt-mKeima is a pH-sensitive mitochondria-targeted fluorescent protein to monitor delivery of mitochondria (440 nm mt-mKeima excitation at neutral pH) to the lysosome (586 nm excitation at acidic pH).[5] A high frequency of mitophagy events was detected in proliferating HDFs in basal conditions (Figure 1A). Specificity of the reporter was validated using a lysosomal inhibitor bafilomycin A1 (Baf A1) (Figure S1A).[15] As mt-mKeima provides only a qualitative snapshot of mitophagy flux, we also employed an alternative mitophagy reporter pSu9-Halo-GFP combined with a fluorescent Halo ligand pulse-labeling, which allows to monitor mitophagy events in real time.[16,17] Using this method, an average of ~90 and up to 300 mitophagy events per cell was recorded over the 48 h period (Figure 1B). These initial observations suggested that primary human skin fibroblasts may rely heavily on mitophagy and provided us with tools to measure changes in mitophagy flux during senescence acquisition.

Senescence was induced by exposing cells to ionizing radiation (IR). Over the course of 11 days post irradiation, cells accumulated the established hallmarks of senescence, including cell cycle arrest, gradual expansion of the mitochondrial network, and an increase in nuclear and overall cell volume (Figures S1B–S1F).[18] Fully developed senescence was also characterized by SA-β-GAL staining and SASP markers interleukin-6 (IL-6) and IL-8 (Figures S1G and S1H). Strikingly, basal mitophagy as measured by mt-mKeima was suppressed as early as 2 h after IR and remained low over the course of 11 days until cells became fully senescent (Figure 1A). Together with the reduced levels of the autophagy proteins p62 and LC3 in mitochondrial fractions isolated from cells 2 h after IR (Figure S1I), this observation indicated that downregulation of mitophagy is an early event in the senescence process.[5] Downregulation of mitophagy in IR-exposed cells was also evident when using the pSu9-Halo-GFP reporter system (Figure 1B).

Developmental Cell
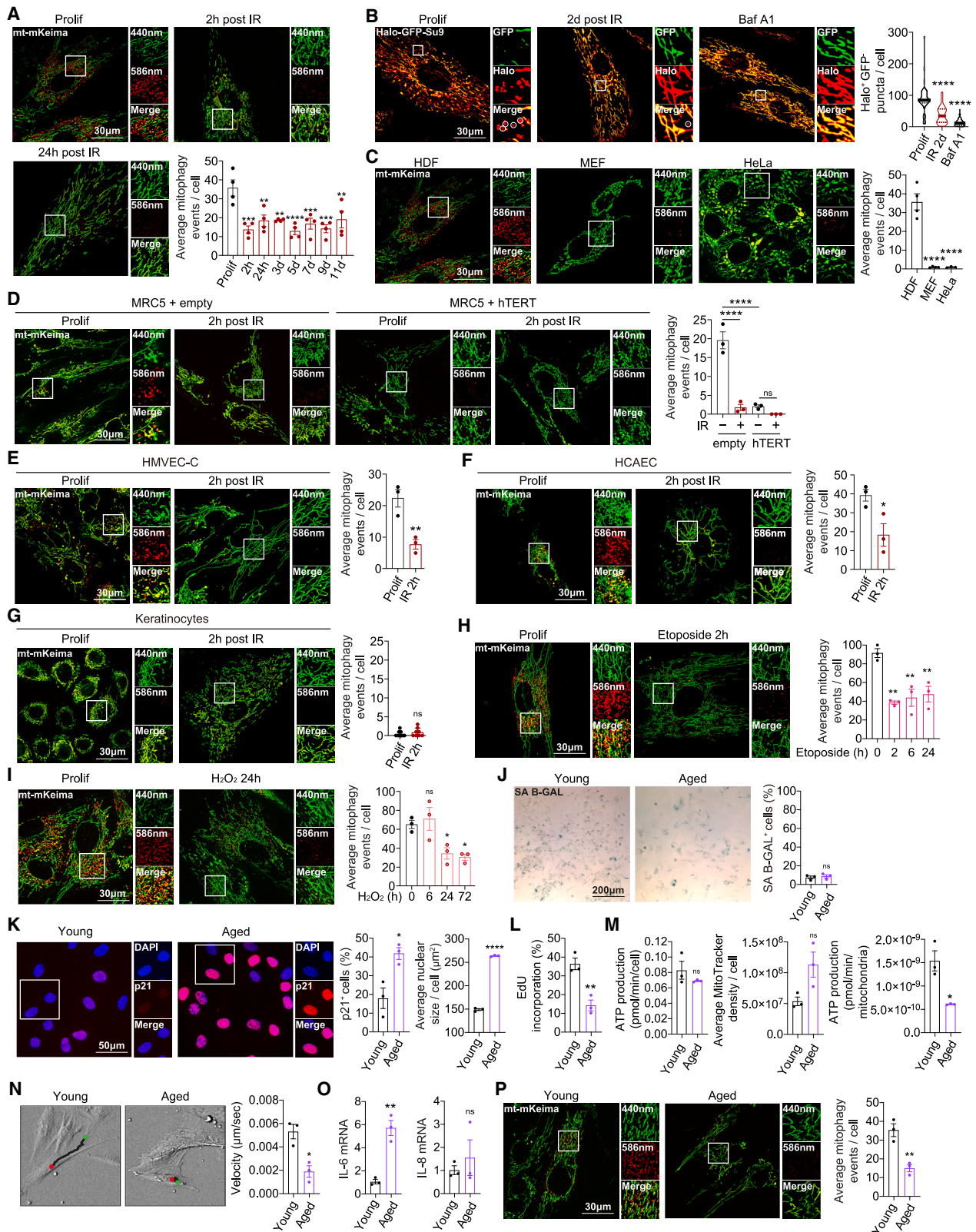## Article

CellPress
OPEN ACCESS

Figure 1. Mitophagy is downregulated in models of cellular senescence and aging

(A) Fluorescence microscopy images and quantifications of mitophagy events (red dots, 586 nm excitation) in HDFs expressing mt-mKeima. Cells were subjected to 20 Gy X-ray irradiation (IR) and imaged at time points as indicated.

(legend continued on next page)

CellPress
OPEN ACCESS

Developmental Cell
Article

Next, we assessed changes in the general autophagy flux during senescence induction using EGFP-RFP-LC3 (LC3 traffic light) reporter visualizing autophagosomes (GFP+RFP+) and their maturation to autolysosomes (GFP−RFP+) (Figures S1J and S1K).[15] High levels of autophagy flux in proliferating HDFs were evident from the predominance of mature autolysosomes in basal conditions. Following IR, autophagy remained functional and further increased during senescence acquisition (Figure S1K). Intact autophagy flux after IR was also confirmed by immunoblotting (Figure S1L) and is consistent with the previously reported role of autophagy in the maintenance of the senescence phenotype.[19–21] We conclude that the early mitophagy downregulation following IR is specific to the turnover of mitochondria and not caused by the general block in the autophagy pathway.

Mitophagy is very low in immortalized or transformed cell lines commonly used in the laboratory,[8,9] and we tested whether high basal mitophagy is a specific feature of primary cells. Indeed, a direct comparison between HDFs and immortalized mouse embryonic fibroblasts (MEFs) or human cervical cancer cell line HeLa indicated a striking difference in mitophagy levels (Figure 1C). Furthermore, immortalization of human lung fibroblasts (MRC5) using human telomerase reverse transcriptase (hTERT)[22] resulted in the suppression of mitophagy, supporting the notion that reliance on basal mitophagy is a feature of primary cells (Figure 1D). High levels of basal mitophagy were also detected in primary human cardiac microvascular endothelial cells (HMVEC-C) and human coronary artery endothelial cells (HCAECs). Similar to HDFs, mitophagy was suppressed in these cell lines following IR (Figures 1E and 1F). At the same time, primary keratinocytes exhibited very low basal mitophagy flux, suggesting cell-type specificity in basal mitophagy rates (Figure 1G). Additionally, the latter observation indicates the lack of correlation between basal mitophagy and the partial oxygen pressure in the tissue of origin (epidermis has been reported as one of the least oxygenated tissues)[23]; therefore, the high basal mitophagy in other primary cell types is unlikely to result from an *in vitro* artifact following exposure to atmospheric oxygen.

Testing different levels of IR indicated that mitophagy suppression occurs at doses required to trigger senescence (Figures S1M and S1N). Therefore, we hypothesized that the shutdown of mitophagy and the following senescence program are induced by a common trigger, such as irreparable DNA damage. Indeed, a decrease in mitophagy events was also observed in alternative models of senescence induction, such as a DNA-damaging drug etoposide or oxidative stress generated by the treatment with hydrogen peroxide (Figures 1H, 1I, S1O, and S1P).[18,24]

Finally, we investigated a model of natural human aging—fibroblasts isolated from skin biopsies of young (≤28 years old) and aged (≥59 years old) donors (3 donors for each age group, Table S1). No elevated SA-β-GAL staining was detected in aged compared with young cells (Figure 1J).[25] However, aged donor fibroblasts were characterized by an increased cell/nuclear size, elevated expression of the cell cycle inhibitor p21, slower proliferation as measured by EdU incorporation, accumulation of mitochondria and impaired mitochondrial function, retardation of cell motility, and changes in the cytokine profile (exemplified by increased levels of IL-6 but not IL-8) (Figures 1K–1O; Table S2). Together, these phenotypes indicated a potential pre-senescence status of cells from aged donors. Interestingly, similar to senescence, mitophagy flux was also significantly reduced in cells from older donors, suggesting that the impairment of mitophagy may also be relevant and contribute to the physiological aging (Figure 1P).

Mitochondria-derived ROS are involved in the induction of mitophagy

Mitophagy is classically triggered by mitochondrial damage, leading to membrane depolarization.[5] However, consistent with previous reports, we found mitochondrial membrane potential to be reduced following IR (Figure S2A),[18] and thus the senescence-associated suppression of mitophagy we observe cannot be explained by the changes in ΔΨm. We recently shown that the increased superoxide generation by the damage to the mitochondrial electron transport chain serves as an alternative cue for the sequestration of mitochondria into autophagosomes.[8,26] Interestingly, using MitoSOX as a mitochondria-targeted superoxide sensor,[27] we detected a striking difference between unstressed cells and following the induction of senescence. Specifically, proliferating cells were characterized by the high fluorescence intensity of MitoSOX foci scattered throughout the mitochondrial network (Figures 2A and 2B). However, subjecting cells to IR or H_2O_2 triggered a significant reduction in MitoSOX-positive mitochondrial puncta (Figures 2A and 2B). The comparison of fibroblasts from young

(B) Confocal microscopy images and quantifications of mitophagy events in HDFs expressing pSu9-Halo-GFP. Cells treated with 1 μM Halo tetramethylrhodamine (TMR) ligand were either subjected to 20 Gy IR or treated with 400 nM bafilomycin A1 (Baf A1, for the last 24 h) and imaged after 2 days.
(C–G) Fluorescence microscopy images and quantifications of mitophagy events in HDF, MEF, and HeLa cells (C), MRC5s and immortalized MRC5s (expressing hTERT) (D), HMVEC-C (E), HCAEC (F), and keratinocytes (G), expressing mt-mKeima. Cells were subjected to 20 Gy IR and imaged after 2 h (D–G).
(H and I) Fluorescence microscopy images and quantifications of mitophagy events in HDFs expressing mt-mKeima and treated with 10 μM etoposide (H) or 10 μM H_2O_2 (I) for the indicated times.
(J–M) Histochemical senescence-associated (SA)-β-GAL staining and quantification of the percentage of cells positive for SA-β-GAL (J), immunostaining for p21 staining and quantifications of the percentage of cells positive for p21 and the average nuclear size (K), and 5-ethynyl-2'-deoxyuridine (EdU) incorporation assay results (L) in human fibroblasts isolated from skin biopsies from three young and three aged donors (see Table S1). (M) Average ATP production per cell, mitochondrial mass assessed by MitoTracker Green staining, and the normalized ATP production to mitochondrial mass in the fibroblasts from donors.
(N) Cell motility assay results in the fibroblasts from donors.
(O) mRNA expression levels of SASP factors, IL-6 and IL-8, in the fibroblasts from donors.
(P) Fluorescence microscopy images and quantifications in the fibroblasts from donors expressing mt-mKeima.
Data are mean ± SEM (A and C–P) or displayed as violin plots (B). *p* values were calculated either by one-way ANOVA, followed by Dunnett's (A–C, H, and I) or Sidak's (D) post hoc analysis, or by unpaired two-tailed Student's t test (E–G and J–P) on three or four (A) independent experiments, or three cell lines per group (J–P). *$p < 0.05$; **$p < 0.01$; ***$p < 0.001$; ****$p < 0.0001$; ns (non-significant).
Scale bars: 30 μm in (A)–(I) and (P), 50 μm in (K), 70 μm in (N), and 200 μm in (J).
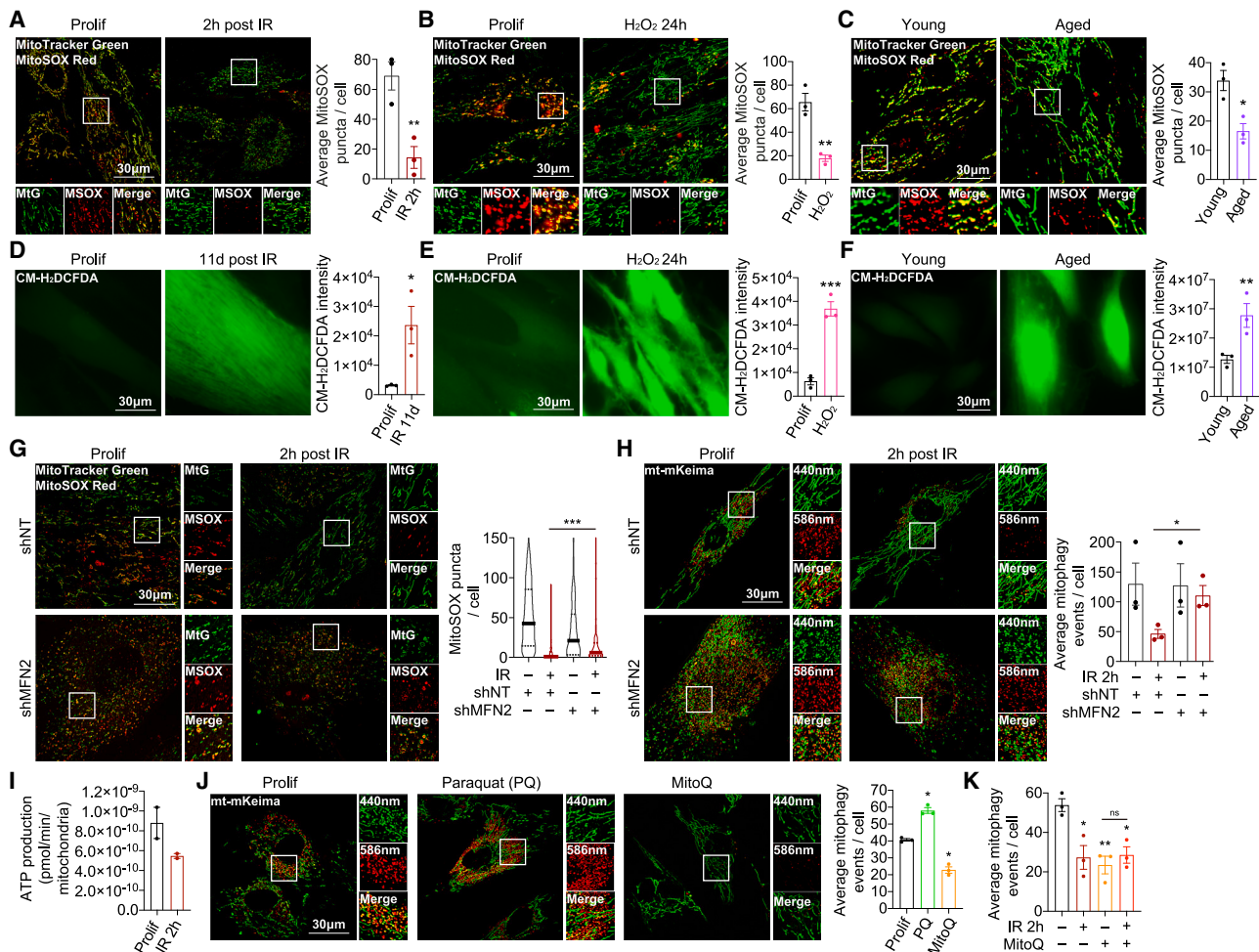See also Figure S1 and Tables S1 and S2.

Figure 2. Mitophagy is triggered by mitochondrial ROS signaling

(A) Fluorescence microscopy images and quantification of the average number of MitoSOX Red puncta in HDFs stained with MitoTracker Green and MitoSOX Red, before and after being subjected to IR.

(B) Fluorescence microscopy images and quantification of the average number of MitoSOX puncta in HDFs stained with MitoTracker Green and MitoSOX Red, treatment with or without H_2O_2 (10 μM) for the indicated times.

(C) Fluorescence microscopy images and quantification of the average number of MitoSOX puncta in human fibroblasts isolated from skin biopsies from young and aged donors and stained with MitoTracker Green and MitoSOX Red.

(D and E) Fluorescence microscopy images and quantifications of CM-H_2DCFDA intensity (ROS indicator) in HDFs, before and after IR (D), or treated with or without H_2O_2 (10 μM) (E).

(F) Fluorescence microscopy images and quantifications of CM-H_2DCFDA intensity in human fibroblasts isolated from skin biopsies from young and aged donors.

(G and H) Fluorescence microscopy images and quantifications of MitoSOX Red puncta (G) and mitophagy events (H) before and after IR in HDFs (G) or mt-mKeima HDFs (H) expressing NT or MFN2 shRNA and stained with MitoTracker Green and MitoSOX Red (G).

(I) Graph representing the average ATP production per cell normalized to mitochondrial mass in HDFs before and 2 h after being subjected to IR (see also Figure S2D).

(J) Fluorescence microscopy images and quantifications of mitophagy events in HDFs expressing mt-mKeima and treated with paraquat (PQ) (15 μM) or MitoQ (10 μM) for 1 h.

(K) Quantification of average mitophagy events in HDFs after treatment with MitoQ (10 μM) and IR.

Data are mean ± SEM (A–F, H, J, and K), mean ± SD (I), or displayed as cell popular violin plot (G). p values were calculated by unpaired two-tailed Student's t test (A–H) or by one-way ANOVA, followed by Dunnett's post hoc analysis (J and K) on three independent experiments. $*p < 0.05$; $**p < 0.01$; $***p < 0.001$; ns (non-significant).

Scale bars: 30 μm.

See also Figure S2.

and older donors indicated a similar downregulation of mitochondrial superoxide levels in aged cells (Figure 2C). These observations were in contrast to the elevated general ROS, a known feature of senescence and aging, in all these models as detected by a fluorescent reporter CM-H_2DCFDA (Figures 2D–2F and S2B).[28]

We speculated that the segregation and accumulation of damaged, superoxide-enriched mitochondria into observable
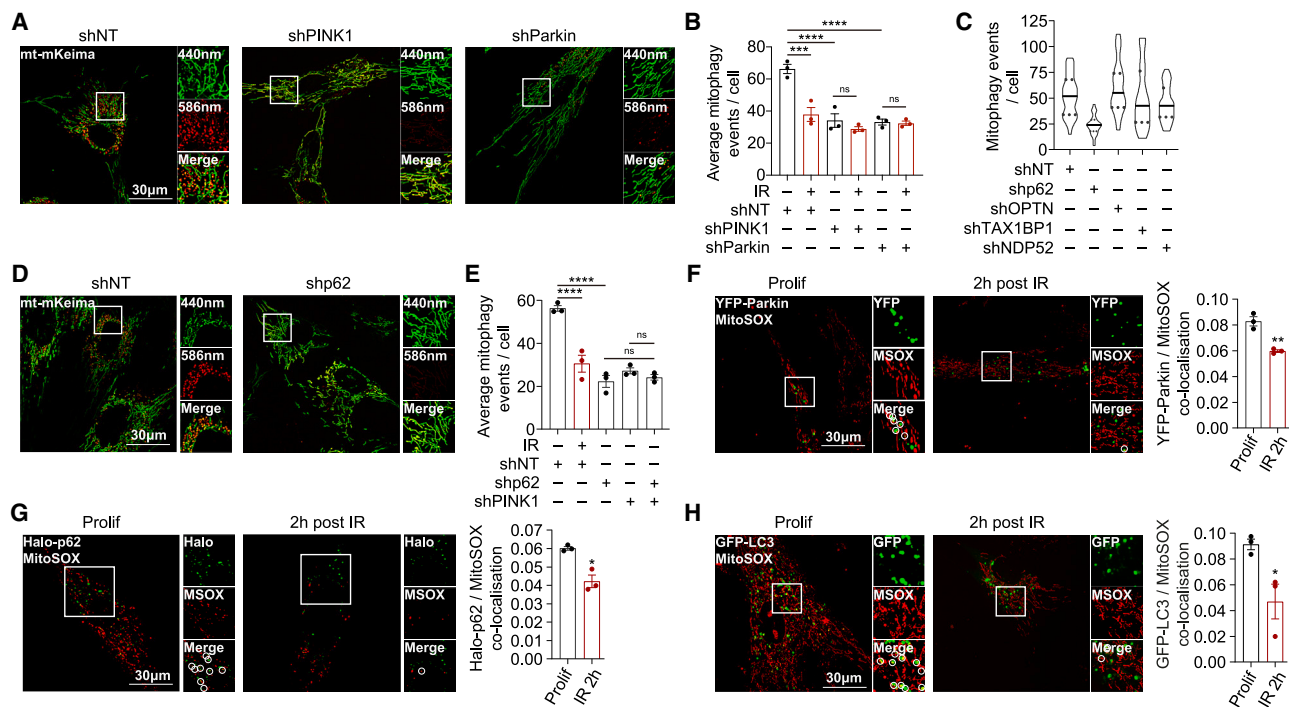
Figure 3. PINK1/Parkin/p62-dependent pathway controls basal mitophagy

(A and B) Fluorescence microscopy images and quantifications of mitophagy events in HDFs expressing mt-mKeima and non-targeting (NT), PINK1, or Parkin shRNA and subjected to IR.

(C) Quantification of average mitophagy events in HDFs expressing mt-mKeima and NT, p62, OPTN, TAX1BP1, or NDP52 shRNA.

(D and E) Fluorescence microscopy images and quantifications of HDFs expressing mt-mKeima and NT or p62 shRNA, as well as PINK1 or both p62 and PINK1 shRNA. HDFs expressing NT shRNA were also subjected to IR.

(F–H) Fluorescence microscopy images of HDFs expressing YFP-Parkin (F), Halo-p62 (G), or GFP-LC3 and stained for MitoSOX Red before and after IR. HDFs expressing Halo-p62 were also stained with 1 μM Oregon Green Halo ligand (G). Graph represents Manders' coefficient quantification of colocalization between YFP-Parkin (F), Halo-p62 (G), or GFP-LC3 (H) and MitoSOX Red.

Data are mean ± SEM (B and E–H) or displayed as cell popular violin plot (C). p values were calculated by one-way ANOVA, followed by Sidak's (B) or Dunnett's (E) post hoc analysis, or by unpaired two-tailed Student's t test (F–H) on three independent experiments. $*p < 0.05$; $**p < 0.01$; $***p < 0.001$; $****p < 0.0001$; ns (non-significant).

Scale bars: 30 μm.

MitoSOX-positive hotspots is prevented by a shift of mitochondrial dynamics toward increased fusion following IR (Figure S1F).[18] To test this hypothesis, we silenced the mitochondrial fusion regulator mitofusin 2 (MFN2), which partially rescued both the MitoSOX puncta and mitophagy levels following IR (Figures 2G, 2H, and S2C). An alternative explanation for the reduced superoxide generation is that mitochondrial respiration is suppressed following irreparable DNA damage, which triggers senescence. Indeed, we observed partial suppression of basal respiration 2 h after IR (Figures 2I and S2D). Additionally, complex I activity, as measured by in-gel assays, was reduced following the treatment of cells with etoposide (Figure S2E). We conclude that both the increased mitochondrial fusion and suppressed respiration could contribute to the disappearance of superoxide-enriched mitochondria seen following senescence induction.

Next, we tested whether physiological signaling from superoxide-enriched mitochondria may serve as a trigger for basal mitophagy. The treatment with paraquat (PQ), which activates mitochondrial superoxide production, increased both the MitoSOX foci frequency and mitophagy levels, while the mitochondria-targeted ROS scavenger mitoquinone (MitoQ) had

the opposite effect (Figures 2J and S2F).[26] Furthermore, mitophagy was suppressed to a similar level after IR or MitoQ treatment with no additive effect when combined, suggesting that both interventions suppress mitophagy via a common mechanism (Figure 2K). Interestingly, repeated exposure of HDFs to MitoQ over the period of 11 days was sufficient to trigger cell cycle arrest and increase the proportion of SA-β-GAL-positive cells (Figure S2G). The latter observation suggests that physiological mitochondrial ROS generation is required to prevent senescence.

In order to further characterize the mechanism of mitophagy deficiency during cellular aging, we had to establish the molecular players controlling basal mitophagy in primary human fibroblasts. Knockdown of PINK1 or Parkin resulted in the suppression of mitophagy down to a level comparable to that observed with IR (Figures 3A, 3B, and S2H). Furthermore, knockdown of PINK1 or Parkin in combination with IR did not result in an additive effect (Figure 3B). Therefore, we concluded that basal mitophagy in primary human fibroblasts is, at least in part, dependent on the function of PINK1 and Parkin. Moreover, following senescence induction, the PINK1/Parkin mitophagy pathway becomes suppressed.

Developmental Cell
Article

Next, we aimed to identify the autophagy receptors involved in basal mitophagy by knocking down those previously implicated in the damage-induced PINK1/Parkin-dependent pathway: OPTN, NDP52, and TAX1BP1 (Figures 3C and S2I).[5] Additionally, we also investigated the role of p62 since mitophagy levels correlated with the recruitment of this prototypic autophagy receptor to mitochondria (Figures 3C–3E and S1I). Interestingly, only knockdown of p62 (using two independent shRNA constructs) resulted in the suppression of basal mitophagy in proliferating HDFs (Figures 3C–3E and S2I–S2K). Simultaneous silencing of p62 and PINK1 did not suppress mitophagy over and above the effect achieved with each shRNA, suggesting that p62 acts within the PINK1/Parkin-dependent mitophagy pathway (Figure 3E).

Finally, to investigate if the superoxide-enriched mitochondria could serve as initiation sites for PINK1/Parkin/p62-dependent basal mitophagy, we performed staining with MitoSOX in the presence of YFP-Parkin and Halo-p62 constructs in proliferating cells and following IR. Both Parkin and p62 showed colocalization with superoxide-enriched mitochondria, which was suppressed following senescence induction, likely due to the reduced frequency of MitoSOX puncta (Figures 3F and 3G). Similarly, colocalization of a general autophagosome marker GFP-LC3 with MitoSOX puncta was also suppressed following IR (Figure 3H). Taken together, we conclude that in primary human fibroblasts, PINK1/Parkin/p62-dependent basal mitophagy targets superoxide-enriched mitochondria for elimination. Importantly, following senescence induction, this process becomes impaired, potentially due to the alteration of the mitochondrial bioenergetics and network dynamics.

Activation of mitophagy reduces markers of senescence
Several pharmacological interventions promoting mitophagy have previously been identified and suggested to have anti-senescence properties. Among these are nicotinamide adenine dinucleotide (NAD) precursors, nicotinamide (NAM), and nicotinamide riboside (NR), as well as the autophagy/mitophagy activator rapamycin.[3,18,20,29,30] We found that the treatment of cells with these molecules efficiently rescued the mitophagy downregulation induced by IR (Figures 4A and S3A). Consistent with the role of superoxide-enriched mitochondria in the initiation of mitophagy, the rescue of mitophagy correlated with partial restoration of MitoSOX foci frequency (Figure 4B). Interestingly, the treatments reduced the frequency of MitoSOX foci in proliferating cells, the reason for which is currently unknown (Figure 4B). Importantly, reactivation of mitophagy by these pharmacological interventions also correlated with the suppression of several senescence markers, without the restoration of cellular proliferative capacity (Figures S3B–S3F).[20,29] At the same time, consistent with the pleiotropic effects of these interventions on cellular physiology and specifically cytokine production,[31,32] we did not observe the rescue of SASP factors IL-6 and IL-8 (Figure S3G).

Next, we tested if activation of mitophagy by NAM, NR, or rapamycin in HDFs requires the PINK1/Parkin/p62-dependent machinery. Treatment with NAM or NR was able to rescue mitophagy defect caused by p62 knockdown (Figure 4C). This result suggested that NAM/NR can override the block caused by the loss of p62, potentially engaging other receptor proteins in a redundant fashion. At the same time, NAM/NR were unable to rescue the mitophagy defect in cells with PINK1 or Parkin knockdown, indicating their strict dependence on the PINK1/Parkin pathway (Figure 4C). Interestingly, rapamycin was able to rescue mitophagy in cells with the loss of PINK1, Parkin, or p62 (Figure 4C). The latter result indicates the existence of additional mechanisms mediating mitophagy in primary human cells with rapamycin being able to engage alternative to the PINK/Parkin-dependent mitophagy pathway(s).

In addition to the suppression of mitophagy as evident 24 h after transduction with PINK1, Parkin, or p62 shRNA constructs (Figures 3A–3E), silencing of these proteins also resulted in cell senescence as assessed 72 h post-transduction (Figures 5A–5D and S4A–S4C). Knockdown of p62 and Parkin also resulted in the elevated IL-6 and IL-8 as SASP markers, as previously reported for models of senescence induced by mitochondrial dysfunction (Figure S4D).[33] Interestingly, senescence resulting from PINK1 knockdown lacked this SASP signature, potentially due to the previously reported role of PINK1 in cytokine expression (Figure S4D).[34] Overall, these data indicated that the loss of basal mitophagy in primary cells is sufficient for the induction of senescence. We combined the above tools to test whether PINK1/Parkin-dependent mitophagy is also necessary for the anti-senescent effects of our pharmacological interventions. Consistent with the PINK1- and Parkin-dependent restoration of mitophagy by NAM and NR (Figure 4C), treatment with these molecules rescued senescence caused by p62 but not PINK1 or Parkin silencing (Figures 5A–5D and S4A–S4C). By contrast, rapamycin treatment that activated mitophagy independent of PINK1, Parkin, or p62 was also able to rescue senescence caused by the silencing of these proteins (Figures 4C, 5A–5D, and S4A–S4C). Together, these data indicate that the loss of mitophagy is sufficient to trigger cellular senescence, while activation of mitophagy is required for the anti-senescence effect of existing pharmacological interventions.

Oligomerization of p62 restores mitophagy and rescues cellular aging phenotypes
We further focused on the mechanism by which p62, which is dispensable for damage-induced PINK1/Parkin-dependent mitophagy, is involved in basal mitophagy in HDFs.[5] Oligomerization of p62 has previously been shown to be required for its function as a SAR.[35] The process of p62 oligomerization can be mediated by the non-covalent interactions of its N-terminal Phox and Bem1 (PB1) domain as well as by disulphide bond formation in response to ROS.[36,37] Taking into account our conclusion that mitochondrial ROS acts as a signal for basal mitophagy in HDFs, we speculated that p62 oxidation and oligomerization on mitochondria may trigger mitophagy initiation. To test this hypothesis, we generated cells where Halo-tagged wild type (WT) or the C105A,C113A oxidation-insensitive mutant p62 constructs were expressed in HDFs followed by silencing of endogenous p62.[36] We also analyzed re-expression of the K7A,D69A p62 mutant which is deficient in PB1 domain-dependent oligomerization but maintains the ability to form disulphide-linked conjugates (DLCs) in response to ROS.[36] The defect of the C105A,C113A (but not K7A,D69A) mutant in the formation of DLC, which are characterized by their sensitivity to a reducing agent, was confirmed by immunoblotting (Figure S5A). Notably,
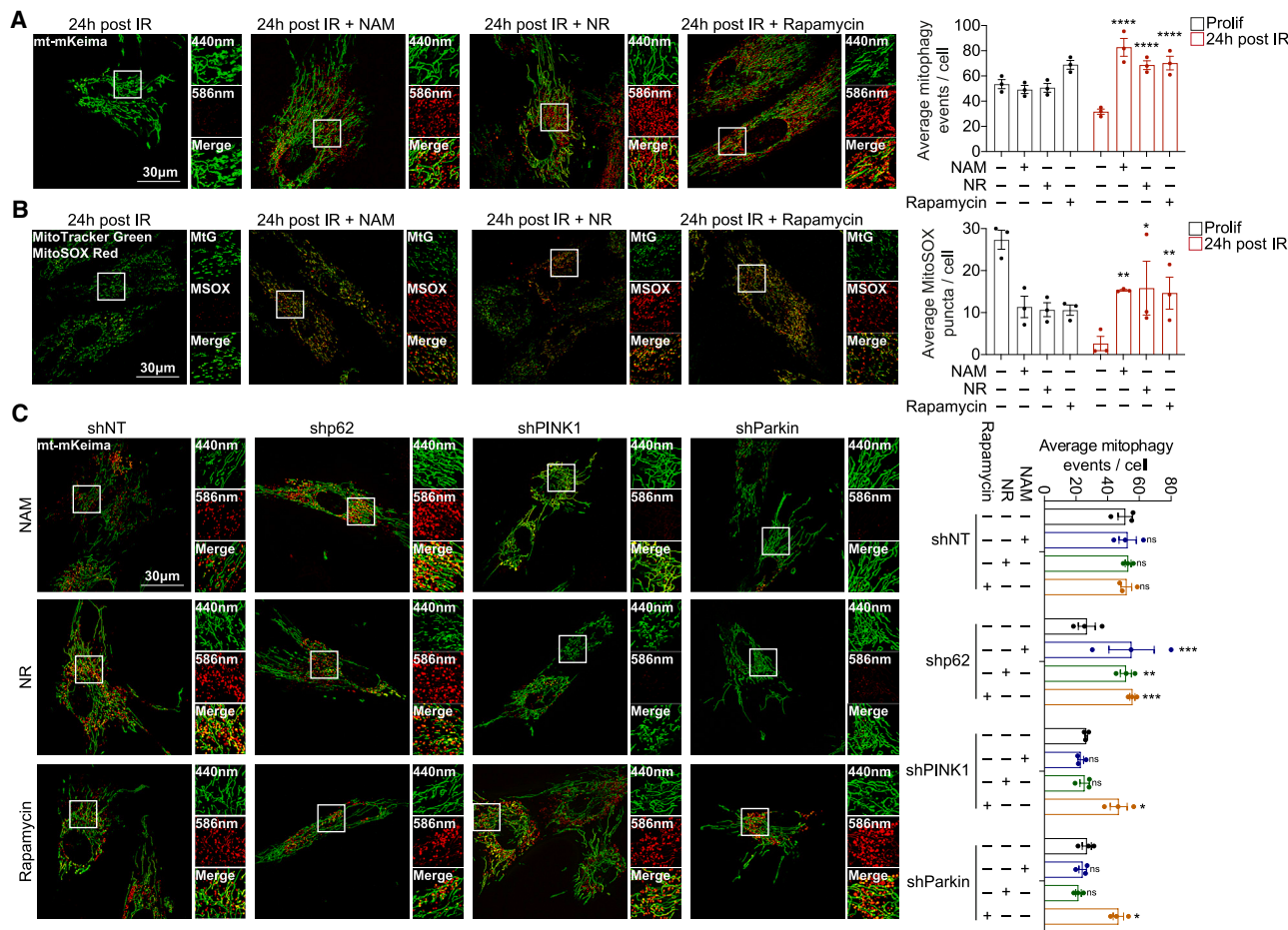
Figure 4. Downregulation of PINK1/Parkin/p62-dependent mitophagy can be rescued by pharmacological interventions

(A) Fluorescence microscopy images and quantifications of mitophagy events in HDFs expressing mt-mKeima. Cells were subjected to IR and treated with NAM (5 mM), NR (5 mM), or rapamycin (10 nM) for 24 h.

(B) Fluorescence microscopy images and quantifications of the average number of MitoSOX Red puncta of HDFs stained with MitoTracker Green and MitoSOX Red in the same conditions as (A).

(C) Fluorescence microscopy images and quantifications of mitophagy events in HDFs expressing mt-mKeima and NT, p62, PINK1, or Parkin shRNA. Cells were treated with NAM (5 mM), NR (5 mM), or rapamycin (10 nM) for 3 days.

Data are mean ± SEM. p values were calculated by two-way ANOVA followed by Dunnett's post hoc analysis on three independent experiments. *$p < 0.05$; **$p < 0.01$; ***$p < 0.001$; ****$p < 0.0001$; ns (non-significant) with respect to corresponding untreated conditions.

Scale bars: 30 μm.

See also Figure S3.

the C105A,C113A (but not K7A,D69A) mutant accumulated on Parkin-positive damaged mitochondria monitored by mt-mKeima and YFP-Parkin reporters in HeLa PentaKO cells lacking 5 endogenous SARs including p62,[5] indicating that lack of ROS sensitivity does not impair the binding of p62 to ubiquitinated cargo (Figure S5B).

Consistent with the role of p62 oligomerization in its function as a mitophagy receptor protein, WT p62 but not oligomerization-deficient C105A,C113A or K7A,D69A constructs rescued the suppression of basal mitophagy caused by p62 knockdown (Figure 6A). Therefore, we next sought to target p62 oligomerization process for mitophagy induction. Natural ligands or small molecules binding ZZ domain of p62 have previously been shown to facilitate DLC formation and stimulate autophagy.[38] We performed an *in silico* screen using a library of 10,800 chem-

ical entities from InterBioScreen collection to identify 25 small molecules that can dock with high affinity into the binding pocket of the ZZ domain of p62 (Figure 6B). The molecules were screened in an *in vitro* cell-based luciferase-p62 degradation assay as a proxy for p62-dependent autophagy (Figures 6C and S5C–S5E).[39] The most potent inducer of p62 degradation, STOCK1N-57534 was tested in orthogonal autophagy assays and found to promote the formation of p62 DLC that accumulated in autophagy-deficient $Atg5^{-/-}$ cells, indicating their turnover by autophagy (Figures 6D and 6E).[40] Furthermore, STOCK1N-57534 treatment also induced the formation of p62- and LC3-positive autophagosomes and increased autophagic flux, as monitored by immunoblotting analyses of cells treated with STOCK1N-57534 in the absence or presence of Baf A1 (Figures S5F and S5G).[15]

Developmental Cell
Article
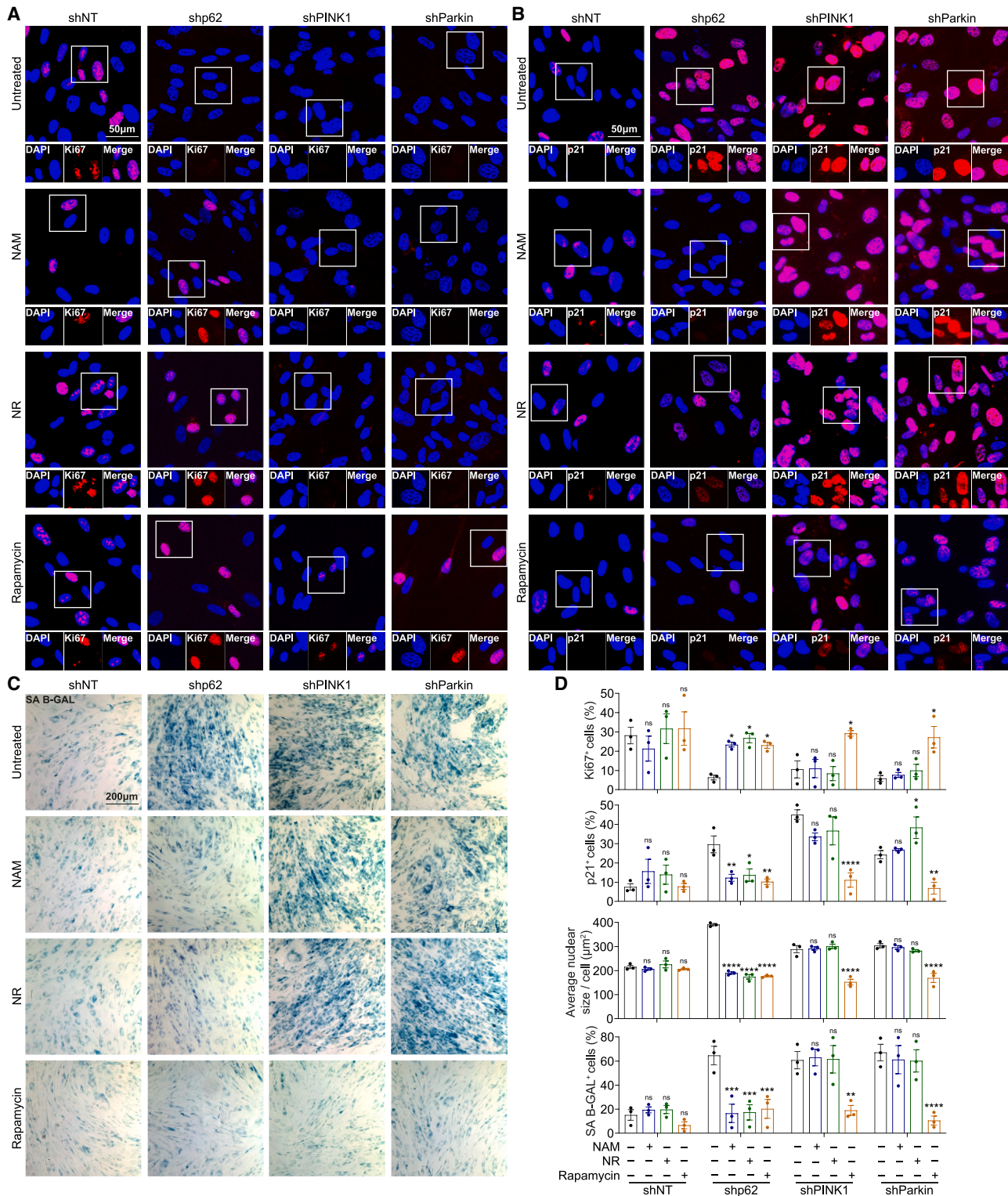
CellPress
OPEN ACCESS

Figure 5. Activation of mitophagy is required to reduce markers of cellular senescence

(A–C) Immunostaining for Ki67 (A), p21 (B), or histochemical SA β-GAL staining (C) in HDFs expressing NT, p62, PINK1, or Parkin shRNA. Cells were treated with NAM (5 mM), NR (5 mM), or rapamycin (10 nM) for 3 days.

(legend continued on next page)

Treatment with STOCK1N-57534 did not increase mitophagy above the level observed in control HDFs or in cells re-expressing WT p62 (Figure 6F). Importantly, the small molecule was unable to rescue the mitophagy impairment in cells with the loss of p62 or with re-expression of C105A,C113A mutant defective in DLC formation. However, the mitophagy defect in cells re-expressing K7A,D69A p62 mutant was efficiently rescued by the treatment with STOCK1N-57534 (Figure 6G). Consistent with the mitophagy measurements (Figures 6A and 6F), the oligomerization-deficient constructs colocalized less with MitoSOX puncta compared with WT p62 (Figure 6G). STOCK1N-57534 treatment did not enhance the colocalization between superoxide-enriched mitochondria and WT or C105A,113A mutant p62, while the treatment induced the colocalization of K7A,D69A p62 with MitoSOX puncta (Figure 6G). The numbers of MitoSOX puncta remained unaffected in all experimental conditions tested (Figure S5H). Together, these data suggest that mitochondria producing high levels of superoxide recruit p62, and its oligomerization, both via disulphide bond formation and PB1 domain interactions, is involved in the initiation of mitophagy. Since K7A,D69A p62 mutant retained the ability to form DLC (Figure S5A), we conclude that the small molecule promotes mitophagy in p62-, and specifically in DLC-dependent manner. Furthermore, since STOCK1N-57534 effect on mitophagy correlated with colocalization of p62 with MitoSOX foci (cf. Figures 6F and 6G), our conjecture is that mitochondria-derived ROS are required for p62 activation in the presence of the small molecule.

Finally, we investigated whether stimulating p62-dependent mitophagy using STOCK1N-57534 can also rescue the mitophagy defect in senescent and naturally aged fibroblasts. Strikingly, a single 5-h treatment with STOCK1N-57534 immediately prior to IR was able to prevent the mitophagy downregulation over the entire 11-day period during senescence acquisition (Figure 7A). Similarly, the low mitophagy in fibroblasts from aged donors was restored to the level of young cells following the treatment with STOCK1N-57534 (Figure 7B). The rescue of mitophagy in cells 11 days after IR was sufficient to partially rescue senescent cell markers: the increased p21 expression (without the rescue of cell cycle arrest), cell/nuclear size, and IL-6/IL-8 levels (Figures 7C, 7D, and S5I). Restoration of the mitophagy levels in fibroblasts from older donors with STOCK1N-57534 was associated with the rescue of increased cell/nuclear size; suppression of elevated p21 and increased cell proliferation; reduction of mitochondrial mass and restoration of mitochondrial function; increase in cell motility; and reduction of IL-6 levels (Figures 7E–7I and S5J).

In conclusion, based on our study using primary human cells, we propose that early suppression of mitophagy is an important driver of the senescence program as well as a feature of physiologically aged cells. Importantly, our studies establish mitophagy as a target for therapeutic interventions aiming to suppress the development of cellular aging phenotypes.

DISCUSSION

Perturbation of protein homeostasis, mitochondrial dysfunction, and cellular senescence are well-established hallmarks of aging.[41] Furthermore, proteostatic pathways such as autophagy are directly involved in the development of senescence phenotypes, indicating extensive mechanistic links between these cellular processes.[12,19,20] However, the role of autophagy in senescence is complex and often viewed as a double-edged sword.[19] Indeed, the loss of protein homeostasis due to autophagy dysfunction can lead to senescence, yet established senescent cells rely on high autophagy flux to maintain their survival and hyperactive metabolism.[12,19] Therefore, understanding the role of specific autophagy pathways such as mitophagy not only provides a mechanistic insight into the nature of the senescence state but also offers an opportunity to identify highly selective targets for the development of anti-aging strategies.[12]

The key challenge when aiming to assess the role of mitophagy is that there is very limited prior knowledge of the molecular mechanisms governing this process in primary human cells. Indeed, the main body of published data on mitophagy is based on stimulating this process by mitochondrial toxins, and the relevance of any molecular players identified in these studies to the mitochondrial quality control by autophagy in the physiological state is largely unknown.[2,4,5] Several findings were made during our efforts to initially identify the molecular factors controlling mitophagy in primary human fibroblasts. First, mitophagy is highly active in basal state in these cells as compared with cancer or immortalized cell lines previously used in mitophagy studies.[5,8–10] The latter cell models show low or even undetectable mitophagy in the absence of triggers such as mitochondrial damage or forced utilization of mitochondrial respiration. It could be speculated that the shift from mitochondrial to glycolytic metabolism during cellular immortalization or transformation removes the dependence on active mitochondrial quality control and making mitophagy disposable.[42] By extension, the relevance of the molecular mechanisms of mitophagy identified in immortalized cell models to the housekeeping mitophagy in primary cells is unknown. Therefore, the second key finding of our study is that PINK1/Parkin-dependent mitophagy mechanism previously believed to be activated only in response to severe mitochondrial damage was found to contribute to the basal mitochondrial turnover in primary human cells.[5] Although recent studies in laboratory animal models cast doubt on the significant contribution of PINK1/Parkin pathway to the mitochondrial turnover *in vivo*,[6,7] our data instead indicate that this mechanism is highly relevant to the mitochondrial quality control in human cells, loss of which is sufficient to trigger senescence. One possible explanation for this apparent discrepancy is an expansion of the repertoire of homeostatic mechanisms in the course of human evolution. Indeed, modifications of the molecular machinery controlling mitophagy, which would improve the ability to respond to stress and maintain cellular function and viability, have most likely contributed to the

---

(D) Graphs represent the percentage of cells positive for Ki67 (A), p21 (B), SA β-GAL (C), and the average nuclear size.

Data are mean ± SEM. *p* values were calculated by two-way ANOVA, followed by Dunnett's post hoc analysis, on three independent experiments. *$p < 0.05$; **$p < 0.01$; ***$p < 0.001$; ****$p < 0.0001$; ns (non-significant) with respect to corresponding untreated condition.

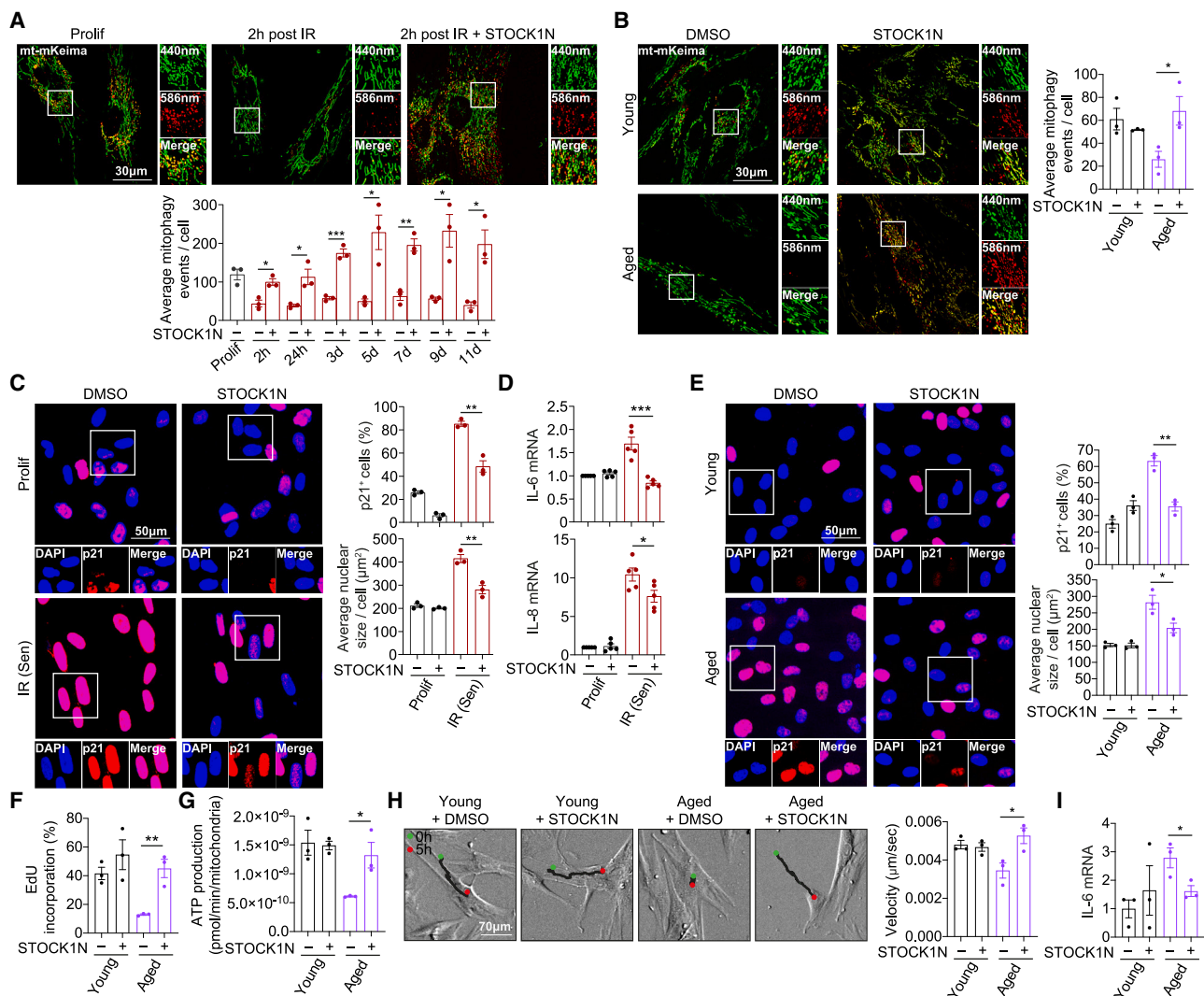Scale bars: 50 μm in (A) and (B) and 200 μm in (C).

See also Figure S4.

Figure 6. p62 oligomerization promotes mitophagy

(A) Fluorescence microscopy images and quantifications of the average mitophagy in HDFs expressing mt-mKeima and non-targeting (NT) or p62 shRNA, as well as wild type (WT), C105A,C113A, or K7A,D69A p62 as indicated.

(B) The docked configuration of STOCK1N (using compound 57534 as an example) in the binding site of p62 ZZ domain as predicted by ChemPLP visualizing *in silico* screening. The ligand occupies the binding pocket, and the protein surface is rendered. Blue depicts a hydrophilic region on the surface; brown depicts hydrophobic region, and gray shows neutral areas.

(C) Diagram of the cell-based small molecule screen.

(D) Chemical structure of STOCK1N-57534.

(E) Immunoblot analyses and quantifications for p62 DLCs formed in $Atg5^{+/+}$ and $Atg5^{-/-}$ MEFs treated with STOCK1N-57534 for 6 h.

(F) Fluorescence microscopy images and quantifications of mitophagy events in HDFs expressing mt-mKeima and NT or p62 shRNA as well as WT, C105A,C113A, or K7A,D69A p62 as indicated, and treated with STOCK1N-57534 (30 μM) for 7 h.

(G) Fluorescence microscopy images of HDFs stained with 1 μM Oregon Green Halo ligand and MitoSOX Red in the same conditions as (F). Graph represents Manders' coefficient quantification of colocalization between Halo-p62 and MitoSOX Red.

Data are mean ± SEM. *p* values were calculated by one-way ANOVA followed by Dunnett's (A) or Sidak's (F and G) post hoc analysis on three (F and G) or five (A) independent experiments. *$p < 0.05$; **$p < 0.01$; ****$p < 0.0001$; ns (non-significant) with respect to p62 shRNA (A) or between the indicated groups.

Scale bars: 30 μm.

See also Figure S5.

Figure 7. p62-dependent small molecule activator of mitophagy rescues cellular aging phenotypes

(A) Fluorescence microscopy images and quantifications of mitophagy events in HDFs expressing mt-mKeima. Cells were treated with STOCK1N-57534 (30 μM) for 5 h prior to 20 Gy IR and imaged at time points as indicated.

(B) Fluorescence microscopy images and quantifications of human fibroblasts isolated from skin biopsies from young or aged donors and expressing mt-mKeima. Cells were treated with STOCK1N-57534 (30 μM) for 7 h.

(C) Immunostaining for p21 and quantifications of the percentage of cells positive for p21 and the average nuclear size in HDFs before and 11 days after IR. Cells were treated with STOCK1N-57534 (30 μM) for 5 h prior to IR and washed after 2 h.

(D) mRNA expression levels of IL-6 and IL-8 in HDFs in the same conditions as (C).

(E) Immunostaining for p21 and quantification of the percentage of cells positive for p21 and the average nuclear size in the fibroblasts isolated from skin biopsies from young or aged donors. Cells were treated with STOCK1N-57534 (30 μM) for 7 h.

(F–I) EdU incorporation assay result (F), ATP production per cell normalized to MitoTracker density (G), cell motility assay results (H), and mRNA expression levels of IL-6 (I), in the same conditions as (E). Note: data of untreated conditions in (G) are from the same experiments as those in Figure 1M.

Data are mean ± SEM. p values were calculated by the multiple t test followed by two-stage linear step-up procedure of Benjamini, Krieger, and Yekutieli (A) or by unpaired two-tailed Student's t test (B–I) on three (A and C) or five (D) independent experiments, or three cell lines per group (B and E–I). *p < 0.05; **p < 0.01; ***p < 0.001.

Scale bars: 30 μm in (A) and (B), 50 μm in (C) and (E), and 70 μm in (H).

See also Figure S5.

increased lifespan of our ancestors.[8,37,43] This conclusion is further supported by the evidence of additional, albeit mechanistically uncharacterized, mitophagy pathways seen in our studies of pharmacological interventions activating mitophagy, suggesting a high complexity of mitochondrial quality control mecha-

nisms mediated by autophagy in physiologically relevant human cells.

Linked to this is the third key observation from our study, the role of mitochondrial ROS signaling as the trigger for mitophagy. This finding is in contrast to the conclusions made from the

Developmental Cell
Article

CellPress
OPEN ACCESS

studies of damage-induced PINK1/Parkin mitophagy mechanisms, where the role of ROS has been highly disputed and remains mechanistically poorly understood.[26] It has to be pointed out that the two manifestations of mitochondrial dysfunction, membrane depolarization and elevated ROS, are mechanistically interconnected, and further studies will be required to precisely delineate the exact sequence of mitochondrial changes acting as a cue for mitophagy activation.[8,42] Interestingly, ROS generation has been shown to be increased in senescence, albeit this increase is concurrent with the expansion of mitochondrial network, which happens relatively late in the senescence program (2 days after IR).[44] Furthermore, we recently proposed that oxidative stress readily observable in senescent cells may come not from mitochondria but cytoplasmic NADH oxidases.[45] It will be important to investigate the changes in cellular and mitochondrial ROS in senescence to further understand the mechanism of persistent suppression of mitophagy as seen in our study.

Our fourth finding is the involvement of p62 as the key receptor in PINK1/Parkin-dependent mitophagy instead of the previously established OPTN, TAX1BP1, and NDP52.[5] Our mechanistic data provide a potential explanation for this observation, where mitochondrial ROS is sensed by p62, which, via oligomerization, increased avidity of interactions with autophagy factors, and cargo clustering, orchestrates mitophagy initiation.[36,46–48] At the same time, this finding is in agreement with data by others indicating that p62 is indeed involved in mitophagy.[49,50] Furthermore, our observation that p62 becomes dispensable when PINK1/Parkin-dependent mitophagy is activated by NAM/NR suggests additional complexity in the use of different SARs in response to specific stimuli activating basal mitophagy in human cells.

Identification of the key molecular factors essential for mitophagy in primary human cells ultimately allowed us to firmly establish the crucial role of mitophagy perturbation in the development of senescence phenotypes.[12] Not only was the mitophagy suppression evident in all models of cellular aging used here, it was also sufficient to trigger the senescence program, while activation of mitophagy was necessary for the anti-senescent effects of pharmacological interventions. Our data indicate that mitochondrial ROS signaling is abruptly shut down upon induction of senescence, which leads to the suppression of mitophagy (but not general autophagy) in the initial stages of senescence acquisition. A similar contrast between selective and global autophagy in the context of DNA damage-induced senescence was also noted previously.[51] Together, these findings bring a novel perspective on the course of events concerning dynamic changes to mitochondria in senescence. Mitophagy suppression might lead to and/or maintain mitochondrial dysfunction, previously shown to constitute an essential element of the senescence program.[12,18,44] Furthermore, mitophagy has emerged as a potential therapeutic target for interventions aiming to suppress the development of senescence and prevent age-related dysfunction. Indeed, our proof-of-concept findings using a small molecule targeting p62 as a mitophagy SAR indicate that normalization of mitochondrial quality control in stressed or aged cells can reverse signs of senescence. Overall, our study provides rationale for the future development of effective and precise means to control mitophagy for the extension of healthy human lifespan.

Limitations of the study

Here we established that several human cell types in culture are characterized by high levels of basal mitophagy, which is important for maintaining mitochondrial homeostasis and preventing senescence. Our initial characterization of the key molecular players controlling the mitophagy process opens a number of questions that could not be addressed in the course of one study. For example, it remains to be investigated why primary but not immortalized cells maintain high rates of mitophagy; how specific mitochondria are selected for degradation; what are the properties of these mitochondria; and how they signal to the mitophagy machinery. Our data point toward the role of mitochondria-derived ROS in this process; however, the exact nature of the mitochondria-cytoplasm retrograde signaling leading to mitophagy activation will require rigorous studies. The mechanisms of p62 DLC formation in response to ROS, as well as how this process is stimulated in the presence of the small molecule STOCK1N-57534, also remain to be established. Furthermore, despite our phenotypic characterization of naturally aged cells, the entire biology underpinning the age-related decline in cellular metabolism and function is an important area for future studies. Finally, our identification of mechanisms specific to primary human cells strongly argues for the need to further develop human-centric cell and tissue models for fundamental and translational aging studies.

STAR★METHODS

Detailed methods are provided in the online version of this paper and include the following:

- KEY RESOURCES TABLE
- RESOURCE AVAILABILITY
  - Lead contact
  - Materials availability
  - Data and code availability
- EXPERIMENTAL MODEL AND STUDY PARTICIPANT DETAILS
  - Cell culture
- METHOD DETAILS
  - Induction of senescence
  - Plasmids
  - Viral transduction
  - Transient transfection
  - Immunoblot analysis
  - Mitochondrial fractionation
  - Fluorescence microscopy
  - Mitophagy assays
  - Immunofluorescence
  - SA β-Galactosidase assay
  - Cell motility assay
  - Assessment of the SASP
  - Seahorse analysis
  - Blue Native electrophoresis and Complex I in-gel activity
  - Mitochondrial network analysis
  - High-throughput screening
- QUANTIFICATION AND STATISTICAL ANALYSIS

SUPPLEMENTAL INFORMATION

Supplemental information can be found online at https://doi.org/10.1016/j.devcel.2024.04.020.

CellPress
OPEN ACCESS

Developmental Cell
Article

REFERENCES

1. Conway, O., Akpinar, H.A., Rogov, V.V., and Kirkin, V. (2020). Selective autophagy receptors in neuronal health and disease. J. Mol. Biol. *432*, 2483–2509. https://doi.org/10.1016/j.jmb.2019.10.013.

2. Sedlackova, L., and Korolchuk, V.I. (2019). Mitochondrial quality control as a key determinant of cell survival. Biochim. Biophys. Acta Mol. Cell Res. *1866*, 575–587. https://doi.org/10.1016/j.bbamcr.2018.12.012.

3. Wilson, N., Kataura, T., Korsgen, M.E., Sun, C., Sarkar, S., and Korolchuk, V.I. (2023). The autophagy-NAD axis in longevity and disease. Trends Cell Biol. *33*, 788–802. https://doi.org/10.1016/j.tcb.2023.02.004.

4. Onishi, M., Yamano, K., Sato, M., Matsuda, N., and Okamoto, K. (2021). Molecular mechanisms and physiological functions of mitophagy. EMBO J. *40*, e104705. https://doi.org/10.15252/embj.2020104705.

5. Lazarou, M., Sliter, D.A., Kane, L.A., Sarraf, S.A., Wang, C., Burman, J.L., Sideris, D.P., Fogel, A.I., and Youle, R.J. (2015). The ubiquitin kinase PINK1 recruits autophagy receptors to induce mitophagy. Nature *524*, 309–314. https://doi.org/10.1038/nature14893.

6. McWilliams, T.G., Prescott, A.R., Montava-Garriga, L., Ball, G., Singh, F., Barini, E., Muqit, M.M.K., Brooks, S.P., and Ganley, I.G. (2018). Basal mitophagy occurs independently of PINK1 in mouse tissues of high metabolic demand. Cell Metab. *27*, 439–449.e5. https://doi.org/10.1016/j.cmet.2017.12.008.

7. Lee, J.J., Sanchez-Martinez, A., Martinez Zarate, A., Benincá, C., Mayor, U., Clague, M.J., and Whitworth, A.J. (2018). Basal mitophagy is widespread in Drosophila but minimally affected by loss of Pink1 or parkin. J. Cell Biol. *217*, 1613–1622. https://doi.org/10.1083/jcb.201801044.

8. Kataura, T., Otten, E.G., Rabanal-Ruiz, Y., Adriaenssens, E., Urselli, F., Scialo, F., Fan, L., Smith, G.R., Dawson, W.M., Chen, X., et al. (2023). NDP52 acts as a redox sensor in PINK1/Parkin-mediated mitophagy. EMBO J. *42*, e111372. https://doi.org/10.15252/embj.2022111372.

9. Kataura, T., Sedlackova, L., Otten, E.G., Kumari, R., Shapira, D., Scialo, F., Stefanatos, R., Ishikawa, K.I., Kelly, G., Seranova, E., et al. (2022). Autophagy promotes cell survival by maintaining NAD levels. Dev. Cell *57*, 2584–2598.e11. https://doi.org/10.1016/j.devcel.2022.10.008.

10. McLelland, G.L., Goiran, T., Yi, W., Dorval, G., Chen, C.X., Lauinger, N.D., Krahn, A.I., Valimehr, S., Rakovic, A., Rouiller, I., et al. (2018). Mfn2 ubiquitination by PINK1/parkin gates the p97-dependent release of ER from mitochondria to drive mitophagy. eLife *7*, e32866. https://doi.org/10.7554/eLife.32866.

11. Dalle Pezze, P., Nelson, G., Otten, E.G., Korolchuk, V.I., Kirkwood, T.B.L., von Zglinicki, T., and Shanley, D.P. (2014). Dynamic modelling of pathways to cellular senescence reveals strategies for targeted interventions. PLoS Comput. Biol. *10*, e1003728. https://doi.org/10.1371/journal.pcbi.1003728.

12. Korolchuk, V.I., Miwa, S., Carroll, B., and von Zglinicki, T. (2017). Mitochondria in cell senescence: is mitophagy the weakest link? EBioMedicine *21*, 7–13. https://doi.org/10.1016/j.ebiom.2017.03.020.

13. Chapman, J., Fielder, E., and Passos, J.F. (2019). Mitochondrial dysfunction and cell senescence: deciphering a complex relationship. FEBS Lett. *593*, 1566–1579. https://doi.org/10.1002/1873-3468.13498.

14. Gorgoulis, V., Adams, P.D., Alimonti, A., Bennett, D.C., Bischof, O., Bishop, C., Campisi, J., Collado, M., Evangelou, K., Ferbeyre, G., et al. (2019). Cellular senescence: defining a path forward. Cell *179*, 813–827. https://doi.org/10.1016/j.cell.2019.10.005.

15. Klionsky, D.J., Abdel-Aziz, A.K., Abdelfatah, S., Abdellatif, M., Abdoli, A., Abel, S., Abeliovich, H., Abildgaard, M.H., Abudu, Y.P., Acevedo-Arozena, A., et al. (2021). Guidelines for the use and interpretation of assays for monitoring autophagy (4th edition)1. Autophagy *17*, 1–382. https://doi.org/10.1080/15548627.2020.1797280.

16. Sun, N., Yun, J., Liu, J., Malide, D., Liu, C., Rovira, I.I., Holmström, K.M., Fergusson, M.M., Yoo, Y.H., Combs, C.A., et al. (2015). Measuring in vivo mitophagy. Mol. Cell *60*, 685–696. https://doi.org/10.1016/j.molcel.2015.10.009.

17. Yim, W.W.Y., Yamamoto, H., and Mizushima, N. (2022). A pulse-chasable reporter processing assay for mammalian autophagic flux with HaloTag. eLife *11*, e78923. https://doi.org/10.7554/eLife.78923.

18. Correia-Melo, C., Marques, F.D.M., Anderson, R., Hewitt, G., Hewitt, R., Cole, J., Carroll, B.M., Miwa, S., Birch, J., Merz, A., et al. (2016). Mitochondria are required for pro-ageing features of the senescent phenotype. EMBO J. *35*, 724–742. https://doi.org/10.15252/embj.201592862.

19. Carroll, B., and Korolchuk, V.I. (2017). Dysregulation of mTORC1/autophagy axis in senescence. Aging (Albany, NY) *9*, 1851–1852. https://doi.org/10.18632/aging.101277.

20. Carroll, B., Nelson, G., Rabanal-Ruiz, Y., Kucheryavenko, O., Dunhill-Turner, N.A., Chesterman, C.C., Zahari, Q., Zhang, T., Conduit, S.E., Mitchell, C.A., et al. (2017). Persistent mTORC1 signaling in cell senescence results from defects in amino acid and growth factor sensing. J. Cell Biol. *216*, 1949–1957. https://doi.org/10.1083/jcb.201610113.

21. Young, A.R.J., Narita, M., Ferreira, M., Kirschner, K., Sadaie, M., Darot, J.F.J., Tavaré, S., Arakawa, S., Shimizu, S., Watt, F.M., and Narita, M. (2009). Autophagy mediates the mitotic senescence transition. Genes Dev. *23*, 798–803. https://doi.org/10.1101/gad.519709.

22. Ahmed, S., Passos, J.F., Birket, M.J., Beckmann, T., Brings, S., Peters, H., Birch-Machin, M.A., von Zglinicki, T., and Saretzki, G. (2008). Telomerase does not counteract telomere shortening but protects mitochondrial function under oxidative stress. J. Cell Sci. *121*, 1046–1053. https://doi.org/10.1242/jcs.019372.

Developmental Cell
Article

23. Ortiz-Prado, E., Dunn, J.F., Vasconez, J., Castillo, D., and Viscor, G. (2019). Partial pressure of oxygen in the human body: a general review. Am. J. Blood Res. 9, 1–14.

24. Wang, Z., Wei, D., and Xiao, H. (2013). Methods of cellular senescence induction using oxidative stress. Methods Mol. Biol. 1048, 135–144. https://doi.org/10.1007/978-1-62703-556-9_11.

25. Costello, L., Dicolandrea, T., Tasseff, R., Isfort, R., Bascom, C., von Zglinicki, T., and Przyborski, S. (2022). Tissue engineering strategies to bioengineer the ageing skin phenotype in vitro. Aging Cell 21, e13550. https://doi.org/10.1111/acel.13550.

26. Sedlackova, L., Kelly, G., and Korolchuk, V.I. (2020). The pROS of autophagy in neuronal health. J. Mol. Biol. 432, 2546–2559. https://doi.org/10.1016/j.jmb.2020.01.020.

27. Robinson, K.M., Janes, M.S., Pehar, M., Monette, J.S., Ross, M.F., Hagen, T.M., Murphy, M.P., and Beckman, J.S. (2006). Selective fluorescent imaging of superoxide in vivo using ethidium-based probes. Proc. Natl. Acad. Sci. USA 103, 15038–15043. https://doi.org/10.1073/pnas.0601945103.

28. Sun, C., Seranova, E., Cohen, M.A., Chipara, M., Roberts, J., Astuti, D., Palhegyi, A.M., Acharjee, A., Sedlackova, L., Kataura, T., et al. (2023). NAD depletion mediates cytotoxicity in human neurons with autophagy deficiency. Cell Rep. 42, 112372. https://doi.org/10.1016/j.celrep.2023.112372.

29. Tan, C.L., Chin, T., Tan, C.Y.R., Rovito, H.A., Quek, L.S., Oblong, J.E., and Bellanger, S. (2019). Nicotinamide metabolism modulates the proliferation/differentiation balance and senescence of human primary keratinocytes. J. Invest. Dermatol. 139, 1638–1647.e3. https://doi.org/10.1016/j.jid.2019.02.005.

30. Fang, E.F., Hou, Y., Lautrup, S., Jensen, M.B., Yang, B., SenGupta, T., Caponio, D., Khezri, R., Demarest, T.G., Aman, Y., et al. (2019). NAD(+) augmentation restores mitophagy and limits accelerated aging in Werner syndrome. Nat. Commun. 10, 5284. https://doi.org/10.1038/s41467-019-13172-8.

31. Cappoli, N., Mezzogori, D., Tabolacci, E., Coletta, I., Navarra, P., Pani, G., and Dello Russo, C. (2019). The mTOR kinase inhibitor rapamycin enhances the expression and release of pro-inflammatory cytokine interleukin 6 modulating the activation of human microglial cells. Excli J. 18, 779–798. https://doi.org/10.17179/excli2019-1715.

32. Nacarelli, T., Lau, L., Fukumoto, T., Zundell, J., Fatkhutdinov, N., Wu, S., Aird, K.M., Iwasaki, O., Kossenkov, A.V., Schultz, D., et al. (2019). NAD(+) metabolism governs the proinflammatory senescence-associated secretome. Nat. Cell Biol. 21, 397–407. https://doi.org/10.1038/s41556-019-0287-4.

33. Wiley, C.D., Velarde, M.C., Lecot, P., Liu, S., Sarnoski, E.A., Freund, A., Shirakawa, K., Lim, H.W., Davis, S.S., Ramanathan, A., et al. (2016). Mitochondrial dysfunction induces senescence with a distinct secretory phenotype. Cell Metab. 23, 303–314. https://doi.org/10.1016/j.cmet.2015.11.011.

34. Zhou, J., Yang, R., Zhang, Z., Liu, Q., Zhang, Y., Wang, Q., and Yuan, H. (2019). Mitochondrial protein PINK1 positively regulates RLR signaling. Front. Immunol. 10, 1069. https://doi.org/10.3389/fimmu.2019.01069.

35. Wurzer, B., Zaffagnini, G., Fracchiolla, D., Turco, E., Abert, C., Romanov, J., and Martens, S. (2015). Oligomerization of p62 allows for selection of ubiquitinated cargo and isolation membrane during selective autophagy. eLife 4, e08941. https://doi.org/10.7554/eLife.08941.

36. Carroll, B., Otten, E.G., Manni, D., Stefanatos, R., Menzies, F.M., Smith, G.R., Jurk, D., Kenneth, N., Wilkinson, S., Passos, J.F., et al. (2018). Oxidation of SQSTM1/p62 mediates the link between redox state and protein homeostasis. Nat. Commun. 9, 256. https://doi.org/10.1038/s41467-017-02746-z.

37. Otten, E.G., Stefanatos, R., Carroll, B., and Korolchuk, V.I. (2018). Oxidation of p62 as an evolutionary adaptation to promote autophagy in stress conditions. Cell Stress 2, 91–93. https://doi.org/10.15698/cst2018.04.132.

38. Cha-Molstad, H., Yu, J.E., Feng, Z., Lee, S.H., Kim, J.G., Yang, P., Han, B., Sung, K.W., Yoo, Y.D., Hwang, J., et al. (2017). p62/SQSTM1/Sequestosome-1 is an N-recognin of the N-end rule pathway which modulates autophagosome biogenesis. Nat. Commun. 8, 102. https://doi.org/10.1038/s41467-017-00085-7.

39. Brown, A., Patel, S., Ward, C., Lorenz, A., Ortiz, M., DuRoss, A., Wieghardt, F., Esch, A., Otten, E.G., Heiser, L.M., et al. (2016). PEG-lipid micelles enable cholesterol efflux in Niemann-Pick Type C1 disease-based lysosomal storage disorder. Sci. Rep. 6, 31750. https://doi.org/10.1038/srep31750.

40. Hosokawa, N., Hara, Y., and Mizushima, N. (2006). Generation of cell lines with tetracycline-regulated autophagy and a role for autophagy in controlling cell size. FEBS Lett. 580, 2623–2629. https://doi.org/10.1016/j.febslet.2006.04.008.

41. López-Otín, C., Blasco, M.A., Partridge, L., Serrano, M., and Kroemer, G. (2013). The hallmarks of aging. Cell 153, 1194–1217. https://doi.org/10.1016/j.cell.2013.05.039.

42. Sedlackova, L., and Korolchuk, V.I. (2020). The crosstalk of NAD, ROS and autophagy in cellular health and ageing. Biogerontology 21, 381–397. https://doi.org/10.1007/s10522-020-09864-0.

43. Ratliffe, J., Kataura, T., Otten, E.G., and Korolchuk, V.I. (2023). The evolution of selective autophagy as a mechanism of oxidative stress response: the evolutionarily acquired ability of selective autophagy receptors to respond to oxidative stress is beneficial for human longevity. BioEssays 45, e2300076. https://doi.org/10.1002/bies.202300076.

44. Passos, J.F., Nelson, G., Wang, C., Richter, T., Simillion, C., Proctor, C.J., Miwa, S., Olijslagers, S., Hallinan, J., Wipat, A., et al. (2010). Feedback between p21 and reactive oxygen production is necessary for cell senescence. Mol. Syst. Biol. 6, 347. https://doi.org/10.1038/msb.2010.5.

45. Fielder, E., Wan, T., Alimohammadiha, G., Ishaq, A., Low, E., Weigand, B.M., Kelly, G., Parker, C., Griffin, B., Jurk, D., et al. (2022). Short senolytic or senostatic interventions rescue progression of radiation-induced frailty and premature ageing in mice. eLife 11, e75492. https://doi.org/10.7554/eLife.75492.

46. Agudo-Canalejo, J., Schultz, S.W., Chino, H., Migliano, S.M., Saito, C., Koyama-Honda, I., Stenmark, H., Brech, A., May, A.I., Mizushima, N., et al. (2021). Wetting regulates autophagy of phase-separated compartments and the cytosol. Nature 591, 142–146. https://doi.org/10.1038/s41586-020-2992-3.

47. Kirkin, V., Lamark, T., Johansen, T., and Dikic, I. (2009). NBR1 cooperates with p62 in selective autophagy of ubiquitinated targets. Autophagy 5, 732–733. https://doi.org/10.4161/auto.5.5.8566.

48. Narendra, D., Kane, L.A., Hauser, D.N., Fearnley, I.M., and Youle, R.J. (2010). p62/SQSTM1 is required for Parkin-induced mitochondrial clustering but not mitophagy; VDAC1 is dispensable for both. Autophagy 6, 1090–1106. https://doi.org/10.4161/auto.6.8.13426.

49. Yamada, T., Murata, D., Adachi, Y., Itoh, K., Kameoka, S., Igarashi, A., Kato, T., Araki, Y., Huganir, R.L., Dawson, T.M., et al. (2018). Mitochondrial stasis reveals p62-mediated ubiquitination in parkin-independent mitophagy and mitigates nonalcoholic fatty liver disease. Cell Metab. 28, 588–604.e5. https://doi.org/10.1016/j.cmet.2018.06.014.

50. Abudu, Y.P., Shrestha, B.K., Zhang, W., Palara, A., Brenne, H.B., Larsen, K.B., Wolfson, D.L., Dumitriu, G., Øie, C.I., Ahluwalia, B.S., et al. (2021). SAMM50 acts with p62 in piecemeal basal- and OXPHOS-induced mitophagy of SAM and MICOS components. J. Cell Biol. 220, e202009092. https://doi.org/10.1083/jcb.202009092.

51. Kang, C., Xu, Q., Martin, T.D., Li, M.Z., Demaria, M., Aron, L., Lu, T., Yankner, B.A., Campisi, J., and Elledge, S.J. (2015). The DNA damage response induces inflammation and senescence by inhibiting autophagy of GATA4. Science 349, aaa5612. https://doi.org/10.1126/science.aaa5612.

52. Hill, D.S., Robinson, N.D.P., Caley, M.P., Chen, M., O'Toole, E.A., Armstrong, J.L., Przyborski, S., and Lovat, P.E. (2015). A novel fully-humanised 3D skin equivalent to model early melanoma invasion. Mol.

Cancer Ther. *14*, 2665–2673. https://doi.org/10.1158/1535-7163.MCT-15-0394.

53. Loftus, S.K., Morris, J.A., Carstea, E.D., Gu, J.Z., Cummings, C., Brown, A., Ellison, J., Ohno, K., Rosenfeld, M.A., Tagle, D.A., et al. (1997). Murine model of Niemann-Pick C disease: mutation in a cholesterol homeostasis gene. Science *277*, 232–235. https://doi.org/10.1126/science.277.5323.232.

54. Kuma, A., Hatano, M., Matsui, M., Yamamoto, A., Nakaya, H., Yoshimori, T., Ohsumi, Y., Tokuhisa, T., and Mizushima, N. (2004). The role of autophagy during the early neonatal starvation period. Nature *432*, 1032–1036. https://doi.org/10.1038/nature03029.

55. Stewart, S.A., Dykxhoorn, D.M., Palliser, D., Mizuno, H., Yu, E.Y., An, D.S., Sabatini, D.M., Chen, I.S.Y., Hahn, W.C., Sharp, P.A., et al. (2003). Lentivirus-delivered stable gene silencing by RNAi in primary cells. RNA *9*, 493–501. https://doi.org/10.1261/rna.2192803.

56. Narendra, D., Tanaka, A., Suen, D.F., and Youle, R.J. (2008). Parkin is recruited selectively to impaired mitochondria and promotes their autophagy. J. Cell Biol. *183*, 795–803. https://doi.org/10.1083/jcb.200809125.

57. Balmer, D., Emery, M., Andreux, P., Auwerx, J., Ginet, V., Puyal, J., Schorderet, D.F., and Roduit, R. (2013). Autophagy defect is associated with low glucose-induced apoptosis in 661W photoreceptor cells. PLoS One *8*, e74162. https://doi.org/10.1371/journal.pone.0074162.

58. Schindelin, J., Arganda-Carreras, I., Frise, E., Kaynig, V., Longair, M., Pietzsch, T., Preibisch, S., Rueden, C., Saalfeld, S., Schmid, B., et al. (2012). Fiji: an open-source platform for biological-image analysis. Nature Methods *9*, 676–682.

59. Berman, H.M., Westbrook, J., Feng, Z., Gilliland, G., Bhat, T.N., Weissig, H., Shindyalov, I.N., and Bourne, P.E. (2000). The Protein Data Bank. Nucleic Acids Res. *28*, 235–242. https://doi.org/10.1093/nar/28.1.235.

60. Valente, A.J., Maddalena, L.A., Robb, E.L., Moradi, F., and Stuart, J.A. (2017). A simple ImageJ macro tool for analyzing mitochondrial network morphology in mammalian cell culture. Acta Histochem. *119*, 315–326. https://doi.org/10.1016/j.acthis.2017.03.001.

61. Wong, K.K.L., Liao, J.Z., Shih, C.R.Y., Harden, N., and Verheyen, E.M. (2020). Hyperpolarized mitochondria accumulate in Drosophila Hipk-over-expressing cells to drive tumor-like growth. J. Cell Sci. *133*, jcs250944. https://doi.org/10.1242/jcs.250944.

62. Bilokapic, S., Maier, T., Ahel, D., Gruic-Sovulj, I., Söll, D., Weygand-Durasevic, I., and Ban, N. (2006). Structure of the unusual seryl-tRNA synthetase reveals a distinct zinc-dependent mode of substrate recognition. EMBO J. *25*, 2498–2509. https://doi.org/10.1038/sj.emboj.7601129.

63. Jones, G., Willett, P., Glen, R.C., Leach, A.R., and Taylor, R. (1997). Development and validation of a genetic algorithm for flexible docking. J. Mol. Biol. *267*, 727–748. https://doi.org/10.1006/jmbi.1996.0897.

64. Verdonk, M.L., Cole, J.C., Hartshorn, M.J., Murray, C.W., and Taylor, R.D. (2003). Improved protein-ligand docking using gold. Proteins *52*, 609–623. https://doi.org/10.1002/prot.10465.

65. Korb, O., Stützle, T., and Exner, T.E. (2009). Empirical scoring functions for advanced protein-ligand docking with PLANTS. J. Chem. Inf. Model. *49*, 84–96. https://doi.org/10.1021/ci800298z.

66. Mooij, W.T.M., and Verdonk, M.L. (2005). General and targeted statistical potentials for protein-ligand interactions. Proteins *61*, 272–287. https://doi.org/10.1002/prot.20588.

Developmental Cell
Article

CellPress
OPEN ACCESS

STAR★METHODS

KEY RESOURCES TABLE

REAGENT or RESOURCE	SOURCE	IDENTIFIER
Antibodies		
α-tubulin	Cell Signaling Technology	Cat#2144; RRID: AB_2210548
β-actin	St John's Laboratory	Cat# STJ96930; RRID: AB_2223172
γH2AX (Phospho-Histone H2A.X)	Millipore	Cat#05-636; RRID: AB_309864
GAPDH	St John's Laboratory	Cat# STJ96931; RRID: N/A
HaloTag	Promega	Cat# G9211; RRID: AB_2688011
Ki67	Abcam	Cat#ab15580; RRID: AB_443209
LC3B (for immunoblotting)	Cell Signaling Technology	Cat#3868; RRID: AB_2137707
LC3B (for immunostaining)	NanoTools	Cat#0260-100; RRID: AB_2943418
MFN2	Sigma-Aldrich	Cat# HPA030554; RRID: AB_10603018
NDP52	Cell Signaling Technology	Cat#60732; RRID: AB_2732810
NDUFS3	Abcam	Cat#ab110246; RRID: AB_10861972
OPTN	Abcam	Cat#23666; RRID: AB_447598
p16	BD Biosciences	Cat#550834; RRID: AB_2078446
p21	Cell Signaling Technology	Cat#2947; RRID: AB_823586
p62 (for immunoblotting)	Progen	Cat#GP62-C; RRID: AB_2687531
p62 (for immunostaining)	MBL	Cat#PM045; RRID: AB_1279301
Parkin	Abcam	Cat#ab77924; RRID: AB_1566559
PINK1	Abcam	Cat#ab23707; RRID: AB_447627
TAX1BP1	Cell Signaling Technology	Cat#5105; RRID: AB_11178939
UQCRC2	Abcam	Cat#ab14745; RRID: AB_2213640
Goat anti-mouse IgG, H&L chain specific peroxidase conjugate	Millipore	Cat#401253; RRID: AB_437779
Goat anti-rabbit IgG, H&L chain specific peroxidase conjugate	Millipore	Cat#401393; RRID: AB_437797
Rabbit anti-guinea pig IgG, peroxidase conjugate	Dako	Cat#P014102; RRID: N/A
Goat anti-mouse IgG (H+L), Alexa Fluor 488	Thermo Fisher Scientific	Cat#A-11001; RRID: AB_2534069
Goat anti-mouse IgG (H+L), Alexa Fluor 594	Thermo Fisher Scientific	Cat#A-11005; RRID: AB_2534073
Goat anti-rabbit IgG (H+L), Alexa Fluor 488	Thermo Fisher Scientific	Cat#A-11008; RRID: AB_143165
Goat anti-rabbit IgG (H+L), Alexa Fluor 594	Thermo Fisher Scientific	Cat#A-11012; RRID: AB_2534079
Chemicals, peptides, and recombinant proteins		
DMEM	Sigma-Aldrich	Cat#D6546
Penicillin/streptomycin	Sigma-Aldrich	Cat#P4333
L-Glutamine	Sigma-Aldrich	Cat#G7513
FBS	Sigma-Aldrich	Cat#F0804
1xMEM non-essential amino acids	Sigma-Aldrich	Cat#M7145
EGM-2 medium	Lonza	Cat#CC-3202
MV2 medium	PromoCell	Cat#C-22121
KGM-2 medium	Lonza	Cat#CC-3107
Geneticin (G418)	Gibco	Cat#11811031
Antimycin A	Sigma-Aldrich	Cat#A8674; CAS: 1397-94-0
Bafilomycin A1	Enzo Life Sciences	Cat#BML-CM110-0100; CAS: 88899-55-2

(Continued on next page)

Continued

REAGENT or RESOURCE	SOURCE	IDENTIFIER
CCCP	Sigma-Aldrich	Cat#C2759; CAS: 555-60-2
Etoposide	Sigma-Aldrich	Cat#E1383; CAS: 33419-42-0
Hydrogen peroxide (H_2O_2)	Sigma-Aldrich	Cat#H1009; CAS: 7722-84-1
Mitoquinone (MitoQ)	Selleckchem	Cat#S8978; CAS: 845959-50-4
Nicotinamide (NAM)	Sigma-Aldrich	Cat#N0636; CAS: 98-92-0
Nicotinamide riboside (NR)	Provided from ChromaDex	N/A
Oligomycin	Merck Millipore	Cat#495455; CAS: 1404-19-9
Paraquat	Sigma-Aldrich	Cat#36541; CAS: 75365-73-0
Rapamycin	Sigma-Aldrich	Cat#R8781
STOCK1N-57534	InterBioScreen	N/A
Lipofectamine 3000	Invitrogen	Cat#L3000015
Lenti-X concentrator	Takarabio	Cat#631232
Polybrene	Sigma-Aldrich	Cat#107689
Puromycin	Gibco	Cat#A1113803
MitoSOX	Invitrogen	Cat#M36008
MitoTracker Green	Invitrogen	Cat#M7514
MitoTracker Deep Red	Invitrogen	Cat#M22426
Tetramethylrhodamine, Methyl Ester, Perchlorate (TMRM)	Invitrogen	Cat#T668
Oregon Green HaloTag ligand	Promega	Cat#G2801
TMR HaloTag ligand	Promega	Cat#G8251
Janelia Fluor 646 HaloTag ligand	Promega	Cat#GA1121
CM-H_2DCFDA	Invitrogen	Cat#C6827
ProLong Gold Antifade Mountant with DAPI	Invitrogen	Cat#P36931
X-Gal solution	Thermo Scientific	Cat#R0941
Critical commercial assays		
Quantibody Human Cytokine Arrays	RayBiotech	Cat#QAH-CYT-1
Deposited data		
Uncropped scan of immunoblot images	This paper	Mendeley data: https://doi.org/10.17632/xxfr7zg66m.1
Experimental models: Cell lines		
HDFn434	Invitrogen	C0045C
Adult dermal fibroblasts, see Table S1	Hill et al.[52]	N/A
MRC5 + empty	Gift from Gabriele Saretzki (Newcastle University)[22]	N/A
MRC5 + hTERT	Gift from Gabriele Saretzki (Newcastle University)[22]	N/A
HMVEC-C	Lonza	CC-7030
HCAEC	PromoCell	C-12221
Keratinocytes	Invitrogen	C0015C
Wild-type MEFs	Gift from Peter Lobel (Rutgers University)[53]	N/A
p62$^{-/-}$ MEFs	Gift from Eiji Warabi (University of Tsukuba)	N/A
Atg5$^{+/+}$ MEFs	Gift from Noboru Mizushima (University of Tokyo)[54]	N/A

Developmental Cell
Article

CellPress
OPEN ACCESS

Continued

REAGENT or RESOURCE	SOURCE	IDENTIFIER
Atg5$^{-/-}$ MEFs	Gift from Noboru Mizushima (University of Tokyo)[54]	N/A
HeLa	European Collection of Cell Cultures	Cat#93021013; RRID:CVCL_0030
PentaKO HeLa	Gift from Michael Lazarou (Walter and Eliza Hall Institute of Medical Research)[5]	RRID:CVCL_C2VN
293FT	Invitrogen	Cat#R70007
Recombinant DNA		
pLV-puro-CMV-Halo-p62	VectorBuilder	https://en.vectorbuilder.com/vector/VB200502-1237wqj.html
pLV-puro-CMV-Halo-p62 C105A,C113A	VectorBuilder	https://en.vectorbuilder.com/vector/VB200502-1246hbf.html
pLV-puro-CMV-Halo-p62 K7A,D69A	VectorBuilder	https://en.vectorbuilder.com/vector/VB200502-1252nem.html
TRC Lentiviral Non-targetting Control shRNA	Horizon	Cat#RHS6848
TRC Lentiviral Human MFN2 shRNA	Horizon	Cat#RHS3979-201909230
TRC Lentiviral Human p62 (SQSTM1) shRNA #1	Horizon	Cat#RHS3979-201739507
TRC Lentiviral Human p62 (SQSTM1) shRNA #2	Horizon	Cat#RHS3979-201739509
TRC Lentiviral Human PINK1 shRNA	Horizon	Cat#RHS3979-201739372
TRC Lentiviral Human Parkin (PRKN) shRNA	Horizon	Cat#RHS3979-201732557
TRC Lentiviral Human OPTN shRNA	Horizon	Cat#RHS3979-201907662
TRC Lentiviral Human TAX1BP1 shRNA	Horizon	Cat# RHS3979-201848526
TRC Lentiviral Human NDP52 (CALCOCO2) shRNA	Horizon	Cat#RHS3979-201848263
psPAX2	Gift from Didier Trono (Ecole Polytechnique Fédérale de Lausanne)	Addgene Plasmid, #12260
pCMV-VSV-G	Gift from Bob Weinberg (MIT)[55]	Addgene Plasmid, #8454
pCHAC-mt-mKeima	Gift from Richard Youle (NIH)[5]	Addgene Plasmid, #72342
YFP-Parkin	Gift from Richard Youle (NIH)[56]	Addgene Plasmid, #23955
pSin-TRE-GW-3xHa-puroR-GFP-LC3	Gift from Raphael Roduit (University of Lausanne)[57]	N/A
pSin-TRE-GW-3xHa-puroR-mRFP-GFP-LC3	Gift from Raphael Roduit (University of Lausanne)[57]	N/A
pMRX-IB-pSu9-HaloTag7-mGFP	Gift from Noboru Mizushima (University of Tokyo)[17]	Addgene Plasmid, #184905
Software and algorithms		
ImageJ/Fiji (version 1.53c)	Schindelin et al.[58]	http://fiji.sc; RRID: SCR_002285
Prism8	GraphPad	http://www.graphpad.com/; RRID: SCR_002798
Huygens Essential	Scientific Volume Imaging	https://svi.nl/HuygensSoftware; RRID: SCR_014237
Scigress (version FJ 2.6)	Fujitsu	https://www.fqs.pl/en/chemistry/products/scigress
GOLD (version 5.2)	CCDC	https://www.ccdc.cam.ac.uk/solutions/software/gold/; RRID:SCR_000188

RESOURCE AVAILABILITY

Lead contact

Further information and requests for resources and reagents should be directed to and will be fulfilled by the lead contact, Viktor I. Korolchuk (viktor.korolchuk@newcastle.ac.uk).

Materials availability

Further information and requests for resources and reagents listed in key resources table should be directed to the lead contact.

Data and code availability

- Uncropped immunoblot images have been deposited at Mendeley and are publicly available as of the date of publication. The DOI is listed in the key resources table. Other data reported in this paper will be shared by the lead contact upon request.
- This paper does not report original code.
- Any additional information required to reanalyse the data reported in this paper is available from the lead contact upon request.

EXPERIMENTAL MODEL AND STUDY PARTICIPANT DETAILS

Cell culture

Primary human cell lines used: foetal dermal fibroblasts (HDF434); adult dermal fibroblasts purchased or isolated in house from surplus human skin as previously described[52] following informed consent (REC reference 19/NE/004_Lovat) (Table S1); foetal lung fibroblasts (MRC5) expressing empty vector or hTERT (gift from Gabriele Saretzki)[22]; cardiac microvascular endothelial cells (HMVEC-C); human coronary artery endothelial cells (HCAEC); keratinocytes. Other cell lines used: wild-type (WT) mouse embryonic fibroblasts (MEFs, gift from Peter Lobel)[53]; $p62^{-/-}$ MEFs (gift from Eiji Warabi); $Atg5^{+/+}$ and $Atg5^{-/-}$ MEFs (gift from Noboru Mizushima)[54]; Human embryonic kidney 293FT; human cervical cancer HeLa and HeLa PentaKO expressing YFP-Parkin and mt-mKeima (gift from Michael Lazarou).[5]

HMVEC-C, HCAEC and keratinocytes were maintained in EGM-2 medium, MV2 medium and KGM-2 medium, respectively. 293 FT cells were cultured in DMEM supplemented with 10% FBS, 100 U/mL penicillin/streptomycin, 2 mM L-glutamine, 1% v/v non-essential amino acids and 400 μg/mL Geneticin (G418). Other cells were cultured in DMEM supplemented with 10% FBS, 100 U/mL penicillin/streptomycin and 2 mM L-glutamine. Cells were maintained in a humidified atmosphere containing 5% CO_2 at 37°C.

Cells were treated with the following compounds at different concentrations and time-points as indicated; etoposide (10 μM), hydrogen peroxide (H_2O_2, 10 μM), bafilomycin A1 (Baf A1, 400 nM), nicotinamide (NAM, 5 mM), nicotinamide riboside (NR, 5 mM), rapamycin (10 nM), paraquat (PQ, 15 μM), Mitoquinone (MitoQ, 10 μM), CCCP (10 μM), STOCK1N-57534 (30 μM), antimycin A (4 μM), oligomycin (10 μM).

See the key resources table for further information of the mammalian cell lines, medium and reagents used in the study.

METHOD DETAILS

Induction of senescence

For stress induced senescence, HDFs were subjected to 20Gy, 10Gy, 5Gy, and 1Gy of X-ray irradiation (IR) using an X-Rad 225 irradiator (Precision X-Ray). Alternatively, cells were treated with H_2O_2 (10 μM) for 3 days, and media was changed with H_2O_2 for a further 3 days. Cells were washed with PBS to terminate treatment.

Plasmids

Plasmids encoding Halo-tagged wild type (WT), oxidation-deficient C105A,C113A or PB1 domain-dependent oligomerisation-deficient K7A,D69A p62 constructs were generated by VectorBuilder using SQSTM1 transcript variant 1 mRNA (NM_003900.5) sequence with silent sequence modifications to ensure resistance to p62 shRNA (Horizon, TRC Lentiviral shRNA TRCN0000007234). Lentiviral vectors (pLKO.1) encoding shRNA (TRC Lentiviral shRNA) against specific targets were purchased from Horizon. pCHAC-mt-mKeima[5] and YFP-Parkin[56] were a gift from Richard Youle. pSin-TRE-GW-3xHa-puroR-GFP-LC3 and pSin-TRE-GW-3xHa-puroR-mRFP-GFP-LC3 were a gift from Raphael Roduit.[57] pMRX-IB-pSu9-HaloTag7-mGFP was a gift from Noboru Mizushima.[17] See the key resources table for further information of plasmids used in the study.

Viral transduction

Stable expression of GFP-LC3, GFP-RFP-LC3, Halo-tagged p62 constructs and shRNA constructs in human dermal fibroblasts was achieved through lentiviral transduction. Lentiviral particles were produced in 293FT cells which were seeded in antibiotic-free medium supplemented with 0.1 mM MEM non-essential amino acids and then co-transfected with lentiviral expression vectors and 2nd generation packaging system plasmids, psPAX2 (gift from Didier Trono) and pCMV-VSV-G (gift from Bob Weinberg)[55] with Lipofectamine 3000 (Invitrogen). After 24 h, media was replaced with fresh media without antibiotics. 48 h after transfection, media from 293FT cells was concentrated using Lenti-X following manufacturer's instructions. Viral transduction was performed on 70% confluent HDFs in the presence of 10 μg/ml Polybrene. Media containing virus was replaced after 24 h with fresh media containing 8 μg/ml of puromycin for selection of transduced cells. Media was replaced every 2–3 days for 10–12 days by keeping the antibiotic selection. Transduced HDFs were then maintained in the presence of lower puromycin concentrations (4 μg/ml) until seeding for experimental purposes. Stable expression of mt-mKeima and pSu9-Halo-GFP in human dermal fibroblasts was achieved through retroviral transduction. Viral particles were produced as described above using retroviral packaging vectors, Gag/Pol (gift from Ian Ganley) and the VSV-G plasmids. See the key resources table for further information of reagents used for viral transduction.

Developmental Cell
Article

CellPress
OPEN ACCESS

Transient transfection

Expression of YFP-Parkin in HDFs was achieved through transient transfection. 2 μg of plasmid was suspended in OptiMEM (Invitrogen, 11058021) with Lipofectamine 3000 following manufacturer instructions. Cells seeded in a 35 mm glass bottom dish (MatTek) were transfected with the mix for 6 h before being replaced with fresh DMEM. Cells were imaged the following day.

Immunoblot analysis

Immunoblotting was performed as described previously.[36] In brief, cells were lysed in RIPA buffer (Sigma-Aldrich) supplemented with 1x Halt™ protease and phosphatase inhibitor cocktail (Thermo Fisher Scientific) and 50 mM N-ethylmaleimide. Protein concentration was measured using DC Protein Assay (Bio-Rad) and samples were prepared by boiling in Laemmli sample buffer (Bio-Rad) in the presence (reduced) or absence (non-reduced) of 2.5% β-mercaptoethanol. Equal amounts of protein (20 – 40 μg) were subjected to SDS-PAGE and transferred to PVDF membranes. Membranes were first blocked in 5% milk (Merck Millipore) in PBS with 1x Tween® 20 (Sigma-Aldrich) for 1 h at room temperature and incubated with primary antibodies overnight at 4C. Secondary antibodies conjugated to horseradish peroxidase (HRP) for rabbit, mouse or guinea pig were used at 1:5000 dilution for 1 h at room temperature. Chemiluminescence detection was achieved using Clarity Western ECL Substrate (Bio-Rad) and a LAS-4000 CCD camera system (Fujifilm). The following primary antibodies were used: guinea pig α-p62 (1:1000), rabbit α-NDP52 (1:1000), rabbit α-OPTN (1:1000), rabbit α-TAX1BP1 (1:1000), mouse α-β-actin (1:5000), rabbit α-LC3 (1:1000), rabbit α-PINK1 (1:1000), mouse α-Parkin (1:1000), mouse α-p16 (1:1000), rabbit α-p21 (1:1000), mouse α-MFN2 (1:1000), mouse α-Halo (1:5000), mouse α-UQCRC2 (1:1,000), mouse α-NDUFS3 (1:1000), rabbit α-Tubulin (1:5000) and mouse α-GAPDH (1:5000). Densitometry analyses of immunoblots were done using Fiji/ImageJ (version 1.48). See the key resource table for further information of antibodies used for immunoblot analysis.

Mitochondrial fractionation

Cells were seeded in 10 cm dishes (5 dishes per condition) and collected with ice-cold PBS by centrifugation for 5 min at 800 g at 4C. Cells were then resuspended in 1 mL fractionation buffer (20 mM HEPES-KOH pH 7.6 (Sigma-Aldrich), 220 mM mannitol (Sigma-Aldrich), 70 mM sucrose (Sigma-Aldrich), 1 mM EDTA (Sigma-Aldrich), 2 mM DTT (Thermo Fisher Scientific) and 0.5 mM PMSF (Sigma-Aldrich)) and homogenised with 50 strokes using a dounce homogeniser (Thermo Fisher Scientific). Cell homogenates were centrifuged for 5 min at 800 g at 4C to pellet cellular nuclei and membrane debris. Supernatant was centrifuged again for 5 min at 800 g at 4C. This step was repeated until no more pellet was present. Small volume (45 μL) of cleared lysate was collected as whole cell lysate, and the rest of lysate were centrifuged for 10 min at 16,100 g at 4C. Supernatant (45 μL) was collected as cytoplasmic fractions, and mitochondria-enriched pellet was washed twice with 1 mL fractionation buffer by centrifugation for 10 min at 16,100 g at 4C. The resulting pellet was resuspended in 450 μL fractionation buffer (10-times dilution) and subjected to immunoblot analysis.

Fluorescence microscopy

Cells seeded in a 35 mm glass bottom dish (MatTek) were stained with 2.5 μM MitoSOX for 1 h and washed three times with cell culture medium. Cells were co-stained with 100 nM Mitotracker Green or 1 μM HaloTag ligand Oregon Green. Halo-tagged p62 constructs in HeLa PentaKO cells were stained with 40 nM Janelia Fluor 646 Halo ligand for 30 min and washed three times with cell culture medium. Co-localisation analysis was performed in Fiji/ImageJ with a macro to remove background followed by calculation of Manders' coefficient. To measure membrane potential, cells were stained with 16.7 nM Tetramethylrhodamine and 100 nM Mitotracker Deep Red for 30 min. CM-H$_2$DCFDA staining was performed according to the manufacturer's instructions.

Fluorescence images were obtained using an LSM700 confocal microscope (Zeiss) and analysis software (Zen 2011, Zeiss), an inverted DM5500 microscope (Leica) or an inverted DMi8 microscope (Leica) with a Plan-Apochromat 63x/1.40 oil immersion lens, equipped with an ORCA-Flash4v2.0 camera (Hamamatsu). Images were deconvolved using Huygens Essential software (version 20.10, Scientific Volume Imaging). Images were analysed in Fiji/ImageJ (version 1.48), and quantification was performed on at least 50 cells per condition. Fluorescence intensity was analysed as outlining single cells as regions of interest and calculation of the raw integrated density value per cell. In autophagy flux assay using mRFP-GFP-LC3 reporter, the number of autophagosomes (GFP$^+$ RFP$^+$ puncta) and autolysosomes (GFP$^-$ RFP$^+$ puncta) per cell were quantified by outlining single cells as regions of interest. See the key resources table for further information of reagents used for fluorescence microscopy.

Mitophagy assays

Cells stably expressing mt-mKeima were seeded in a 35 mm glass bottom dish (MatTek). The live-cell mt-Keima signal was obtained via widefield microscopy using the DMi8 and 2 filtersets to obtain the acidic (561 nm excitation, "red") and pH-neutral (480 nm, "green") mKeima signals. Using FIJI/ImageJ, a macro was applied to the mt-mKeima signal to extract mitolysosomes. In detail, images were masked by applying MaxEntropy threshold to the images obtained with 561 nm excitation to remove low mt-mKeima red signal and background. Then, images were generated by subtracting the signal of green mKeima from that of red mKeima. Resulting images were binarised with the MaxEntropy threshold algorithm to extract mitolysosomes. Mitophagy events were determined as the number of puncta per cell.

Cells stably expressing pSu9-Halo-GFP seeded in a 35 glass bottom dish (MatTek) were stained with 1 μM Halo TMR ligand for 48 h. Fluorescence images were obtained using an LSM700 confocal microscope (Zeiss). The number of mitolysosomes (GFP$^-$ Halo$^+$ puncta) per cell was quantified using Fiji/ImageJ. See the key resources table for further information of reagents used for mitophagy assays.

Immunofluorescence

Immunofluorescence analyses were performed as described previously.[36] In brief, cells were seeded on coverslips in 24-well plates and fixed in 4% formaldehyde in PBS for 10 min at room temperature followed by permeabilisation in 0.5% Triton X-100 (Sigma-Aldrich) in PBS for 4 min at room temperature (Ki67 and p21) or in methanol for 4 min at -20 °C (LC3 and p62). Cells were then blocked for 1 h in 5% normal goat serum (Sigma-Aldrich) in PBS at room temperature and incubated with primary antibodies overnight at 4°C. Cells were washed three times and incubated with the appropriate secondary antibodies for 1 h at room temperature. Cells were washed, and coverslips were mounted on slides with Prolong Gold antifade mountant with DAPI (Invitrogen). Fluorescence images were obtained as described above. The following primary antibodies were used: rabbit α-Ki67 (1:250), rabbit α-p21 (1:1000), mouse α-LC3 (1:200) and rabbit α-p62 (1:500). See the key resources table for further information of antibodies used for immunofluorescence.

SA β-Galactosidase assay

Cells were seeded on coverslips in 24-well plates. Cells were fixed with 4% formaldehyde in PBS for 10 min. Fixed cells were washed three times with PBS, before adding to each well 0.5 ml of prewarmed X-Gal staining solution (2 mM $MgCl_2$, 5 mM $K_4Fe(CN)_6 \cdot 3H_2O$, 5 mM $K_3Fe(CN)_6$, 1 mg/ml X-Gal solution ready to use (R0941, Thermo Fisher Scientific) in PBS). Plates were incubated for 24 h at 37 °C, washed, mounted and imaged. SA-β-Gal activity positive and negative cells were quantified using FIJI/ImageJ.

Cell motility assay

Cells were seeded in glass bottomed multiwell plates (Greiner, 662892), 24 h prior to imaging. Images were captured using a Zeiss CellDiscoverer 7 with a 5x/0.35NA lens with a 2x optovar using oblique mode brightfield with a Hamamatsu Fusion camera every 300 seconds for 5 h (1 ms exposure time), capturing 2 random fields per well. Cells were maintained at 37°C, 5% CO_2 throughout experiments. 6 cells were analysed per field using the Manual Tracking plugin in Fiji/ImageJ and shown as mean movement per cell recorded.

Assessment of the SASP

Quantibody Human Cytokine Arrays for 20 cytokines (RayBiotech; QAH-CYT-1) were performed using 24 h conditioned media collected from primary dermal fibroblast cultures (Table S1). P and adjusted P (Q) values were calculated by multiple t-test with false discovery rate approach using two-stage linear step-up procedure of Benjamini, Krieger and Yekutieli, using Prism 8.4.3 software (GraphPad).

mRNA levels of human IL-6 and IL-8 were measured by qPCR. Total RNA was extracted using RNeasy Mini Kit (QIAGEN, 74104). From 500 ng of total RNA, first-strand complementary DNA (cDNA) was produced using SuperScript III reverse transcriptase (Invitrogen, 18080044) according to the manufacturer's instructions. Quantitative PCR was performed in a StepOnePlus Real-Time PCR system (Applied Biosystems) using Power SYBR Green PCR Master Mix (Applied Biosystems, 4367659). mRNA expression levels were determined with the ΔΔCt method and normalised to GAPDH levels. Sequences of the primers used are as follows: IL-6, CAGGAGCCCAGCTATGAACT and GAAGGCAGCAGGCAACAC; IL-8, GAGTGGACCACACTGCGCCA and TCCACAACCCTCTGCACCCAGT; GAPDH, AAATCCCATCACCATCTTCC and GACTCCACGACGTACTCAGC.

Seahorse analysis

The Seahorse XF Cell Mito Stress Test Kit (Agilent) was used to measure oxygen consumption rates in HDF434 or adult dermal fibroblasts (Table S1). One day prior to the assay cells were seeded at either 4000 per well (HDF434, donor IDs: 14610f, 1534331, 1643551) or 3000 per well (donor IDs: 693503, 2877f, 2905f). Where indicated, HDF434 plates were subjected to 20Gy IR 2 h before assay. STOCK1N (30 μM) or vehicle (DMSO) treatments were performed 7 h before Seahorse assays using adult dermal fibroblasts. Cells were stained with 100 nM Mitotracker Green for mitochondrial density measurement.

The Mito Stress Test was performed as per manufacturer's guidelines on a Seahorse XF96 Extracellular Flux analyser using previously optimised conditions. Following assay completion, cells were fixed in 4% PFA for 20 minutes. PFA was then removed, and cells were washed twice with PBS. Following fixation, cells were stained with Hoescht nucleic acid stain (Invitrogen) for 10 min before being washed twice in PBS. Fluorescence was subsequently measured using the PHERAstar FSX plate reader (BMG LABTECH) at 350/460nm for normalisation purposes. Following normalisation, OCR measurements were interpreted from data generated from the Agilent Seahorse Wave software version 2.6.3.5. Basal respiration data in unstressed conditions is presented. OCR measurements were further normalised to mitochondrial density to obtain ATP production (pmol/min/mitochondria).

Blue Native electrophoresis and Complex I in-gel activity

HDF treated with 10 μM etoposide for 2 h were collected by trypsinization and resuspended in 20 mM HEPES pH 7.6, 220 mM mannitol, 70 mM sucrose, 1 mM EDTA, 0.2% fatty acid-free BSA buffer. Upon 20 minutes incubation in the buffer, cells were homogenized using Dounce Glass Homogenizer. Concentration of protein in mitochondrial isolates was determined with Bradford reagent (Sigma-Aldrich). Equal amounts of mitochondria (20 μg) were lysed for 15 min on ice in 0.625% digitonin and subsequently centrifuged for 30 min at 20,000 × g, 4 °C. Coomassie G-250 was added to the sample at the concentration of 0.25%. Mitochondrial complexes were resolved with Blue Native PAGE using the 4–16% NativePAGE Novex Bis-Tris Mini Gels (Invitrogen) in a Bis-Tris/Tricine buffer. Cathode buffer initially contained 0.02% G-250 followed by the 0.002% G-250. A set of separated mitochondrial complexes

was subjected to Complex I in-gel activity assay. Activity was measured by incubating BN-PAGE gel in NADH 0.1 mg/ml and nitro-tetrazolium blue 2.5 mg/ml in 5 mM Tris (pH 7.4). Image of the proceeding reaction was taken every 5 minutes for the following hour. A set of separated mitochondrial complexes were transferred onto a polyvinylidene fluoride membrane using the wet transfer methanol-free system. The membrane was immunodecorated with NDUFS2 antibody (Abcam, ab96160, 1:1000), followed by ECL-based signal detection. Signal obtained by Complex I activity assay was normalized to the levels of fully assembled Complex I using Fiji software.

Mitochondrial network analysis
Mitochondrial morphologies in deconvolved mt-mKeima green (480 nm excitation) images were quantified using the Stuart lab Mitochondrial Network Analysis (MiNA), ImageJ plugin.[60] Raw images were pre-processed via deconvolution prior to analysis. The MiNA parameters selected include those previously published,[61] plus the addition of Ridge Detection: High contrast 5, Low contrast: 0, Line width: 12. Line length: 12.

High-throughput screening
For *in silico* screening p62-targeting small molecules, 10,800 compounds from the InterBioScreen Ltd natural product-collection were docked to the binding pocket of p62 ZZ domain (PDB ID: 5YP8, resolution 1.448 Å)[62] which was obtained from the Protein Data Bank (PDB).[59] The Scigress version FJ 2.6 program was used to prepare the crystal structure for docking, i.e., hydrogen atoms were added, the co-crystallised ligand, Arg-peptide was removed as well as crystallographic water molecules. The centre of the binding pocket was defined as a side chain carbonyl carbon of Asp23 (x = 8.242, y = -14.427, z = 197.93) with a radius of 10 Å. Two known inhibitors XIE62-1004 and XIE2008A were first docked into the binding site and their scores shown in Table S3 were used as a guide. For the initial screen 30% search efficiency was used (virtual screen) with ten runs per compound. For the second phase (re-dock) 100% efficiency was used in conjunction with fifty docking runs. The GoldScore(GS)[63] and ChemScore(CS),[64] improved Piecewise Linear Potential (ChemPLP)[65] and Astex Statistical Potential (ASP)[66] scoring functions were implemented to validate the predicted binding modes and relative energies of the ligands using the GOLD v5.2 software suite.

STOCK1N compounds identified as p62 binders *in silico* (Table S3) were purchased from InterBioScreen Ltd and screened in cells expressing TET-inducible p62-fluc construct as previously described.[39] In brief, p62-fluc-expressing MEFs were plated into white 96 well plates (2,000 cell/well with 100 μl media) and allowed to settle for 24 h. Next, the MEFs were treated with 1 μg/ml doxycycline (Sigma-Aldrich 33429) for 24 h before being rinsed 3 times with PBS. Subsequently, cells were treated with STOCK1N compounds for 48 h in normal growth medium and analysed using ONE-Glo™ + Tox Luciferase Reporter and Cell Viability Assay (Promega) by following the manufacturer's protocol.

QUANTIFICATION AND STATISTICAL ANALYSIS

Graphical data denote the mean ± s.e.m (of n = 3 or more biological replicates) and are depicted by column graph scatter dot plot or displayed as cell popular violin plots using Prism 8.4.3 software (GraphPad). *P* values were determined by Student's t test (two-tailed, unpaired) between two groups, one-way or two-way ANOVA, followed by Dunnett's or Sidak's post-hoc analysis, or multiple t-test with false discovery rate approach using two-stage linear step-up procedure of Benjamini, Krieger and Yekutieli, using Prism 8.4.3 software (GraphPad), unless otherwise stated. A *P* value < 0.05 was considered significant. *, $P<0.05$; **, $P<0.01$; ***, $P<0.001$; ****, $P<0.0001$; ns (non-significant).